Depth-partitioning of particulate organic carbon composition in the rising and falling stages of the Amazon River

Sarah Z. Rosengard[1,2,3*], Jose Mauro S. Moura[4], Robert G.M. Spencer[5], Carl Johnson[1], Ann McNichol[6], Andrew D. Steen[7], and Valier Galy[1]

1. Department of Marine Chemistry and Geochemistry, Woods Hole Oceanographic Institution, Woods Hole, MA, USA
2. Department of Earth, Atmospheric and Planetary Sciences, Massachusetts Institute of Technology, Cambridge, MA, USA
3. Department of Liberal Arts, The School of the Art Institute of Chicago, Chicago, IL, USA*
4. Programa de Pós-Graduação em Recursos Naturais da Amazônia, Universidade Federal do Oeste do Pará, Santarém, Pará, Brazil
5. Department of Earth, Ocean & Atmospheric Science, Florida State University, Tallahassee, FL, USA
6. Department of Marine Geology and Geophysics, Woods Hole Oceanographic Institution, Woods Hole, MA, USA
7. Departments of Microbiology and Earth and Planetary Sciences, University of Tennessee, Knoxville, TN, USA

*Corresponding author's current affiliation

Key points

- Amazon River suspended sediments show little variation in organic carbon composition with depth, despite hydrodynamic sorting.
- Estimated particulate organic carbon fluxes range from 370 to 540 kilograms per second between rising and falling stages.
- The majority of Amazon River particulate organic carbon exported from the mainstem at Óbidos is soil-derived.

Abstract

The Amazon River mobilizes organic carbon across one of the world's largest terrestrial carbon reservoirs. Quantifying the sources of particulate organic carbon (POC) to this flux is typically challenging in large systems like the Amazon River due to hydrodynamic sorting of sediments. Here, we analyze the composition of POC collected from multiple total suspended sediment (TSS) profiles in the mainstem at Óbidos, and surface samples from the Madeira, Solimões and Tapajós Rivers. As hypothesized, TSS and POC concentrations in the mainstem increased with depth and fit well to Rouse models for sediment sorting by grain size. Coupling these profiles to Acoustic Doppler Current Profiler discharge data, we estimate a large decrease in POC flux (from 540 to 370 kilograms per second) between the rising and falling stages of Amazon River mainstem. The C/N ratio, stable and radiocarbon signatures of bulk POC are less variable within the cross-section at Óbidos, and suggest that riverine POC in the Amazon River is predominantly soil-derived. However, smaller shifts in these compositional metrics with depth, including leaf wax *n*-alkanes and fatty acids, are consistent with the perspective that deeper and larger particles carry fresher, less degraded organic matter sources (i.e., vegetation debris) through the mainstem. Overall, our cross-sectional surveys at Óbidos highlight the importance of depth-specific sampling for estimating riverine export fluxes. At the same time, they imply that this approach to sampling is perhaps less essential with respect to characterizing the composition of POC sources exported by the river.

Plain language summary

The Amazon River transports one of the largest quantities of freshwater organic carbon into the Atlantic Ocean. In this study, we collected suspended particles at different depths within a cross-section of the Amazon River mainstem, during the rising and falling stages of the river's hydrological cycle. We analyzed the organic carbon, nitrogen, grain size, and leaf-derived compounds in these particles, and integrated water velocity measurements to calculate the quantity of carbon in particle form moving through the river at these two stages. The analyses showed that large, dense particles concentrate with depth in the Amazon River mainstem. The composition of these particles is relatively homogenous, but slight variations in metrics like carbon-to-nitrogen ratio, age derived from carbon-dating, and leaf waxes imply that less degraded sources of organic carbon are found in the deeper and coarser grained particles.

Overall, the data suggest that the majority of Amazon River particulate organic carbon comes from a mixture of soil organic carbon washing in from different landscapes and soil depth horizons. A small but globally significant quantity of this carbon will get buried in the deep Atlantic Ocean, forming a long-term carbon sink.

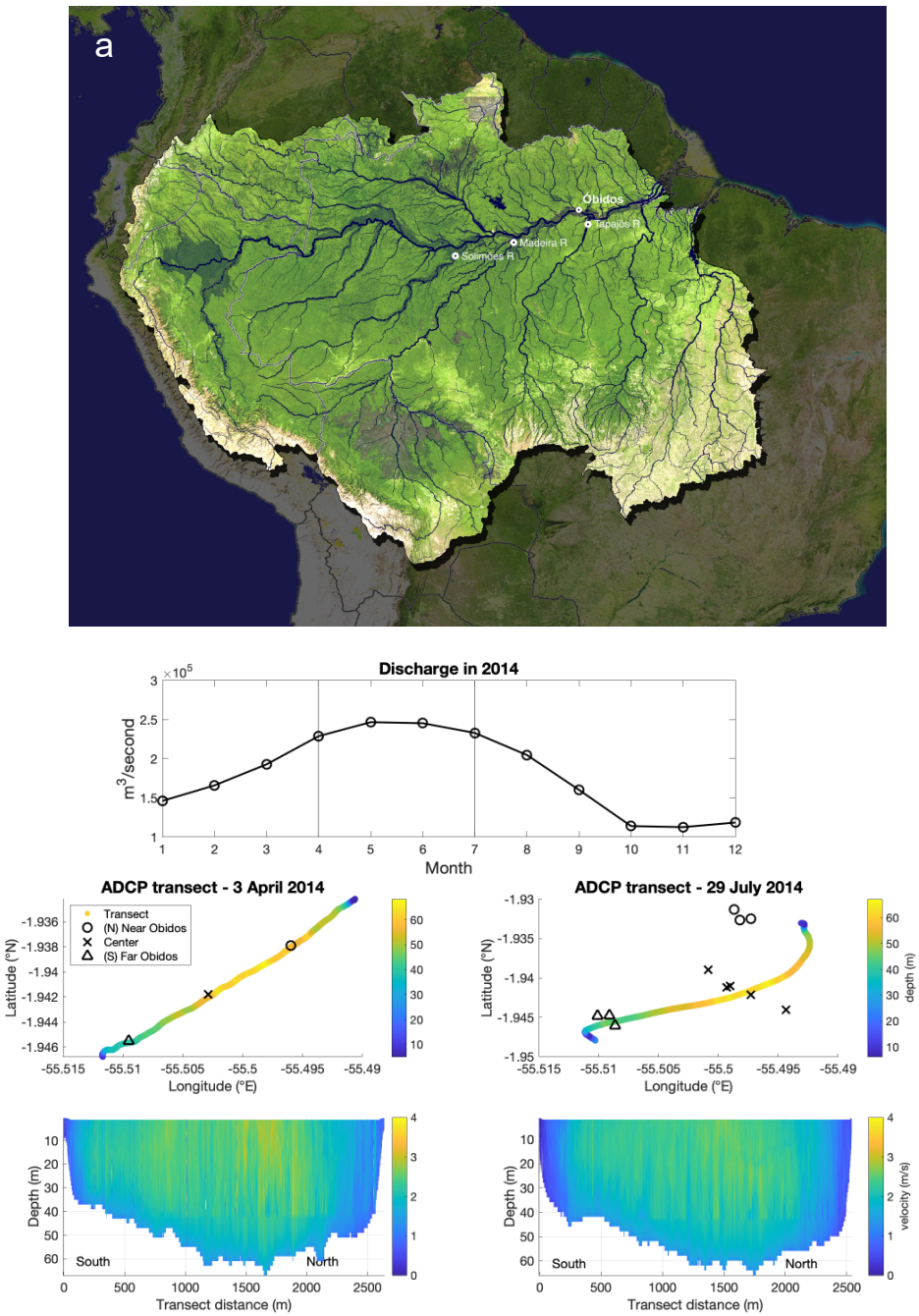

Figure 1. Top row (a): the Amazon River Basin and all field sites from June 2005, April 2014 and July 2014. Image credit: Paul Lefebvre and Greg Fiske (Woods Hole Research Center). Second row from top:

monthly mainstem discharge time-series in 2014, compiled by the Brazilian Agência Nacional de Águas (https://www.snirh.gov.br/hidroweb/serieshistoricas). Each number represents the average flow measured on the first day of each month of the year (month #1 is January; month #12 is December). The vertical solid lines represent the two sampling months, April and July. Third row from top: Acoustic Doppler Current Profiler (ADCP) transects in latitude/longitude across the Amazon River at Óbidos in April and July 2014, with color indicating river depth. Transects started at the right bank across from Óbidos, and ended at the left bank near Óbidos. The markers indicate approximate locations of each TSS sample. Note that exact GPS coordinates of each individual sample were not recorded during the April transect. Bottom row: measured and extrapolated water velocities within the cross-section at Óbidos in April 2014 and July 2014, with the colorbar representing water velocity.

1 Introduction

The Amazon River Basin, a global biodiversity hotspot, is one of the largest reservoirs of biospheric organic carbon on the planet. The river network includes eight major tributaries that extend across a six million square kilometer drainage basin. Torrential seasonal rains mobilize massive quantities of suspended sediments across flooded and upland rainforests, drier savannah, high-elevation Andean landscapes, as well as cropland and pasture, into the tributaries and mainstem. As a result, the Amazon River sustains the highest freshwater discharge (Dai & Trenberth, 2002) and one of the largest export fluxes of suspended sediments and particulate organic carbon (POC) to the ocean globally (see compilation by Galy et al., 2015). The Amazon River Basin's role as a major conduit for POC transport from land to sea has motivated decades of research into its influence on the global carbon cycle and long-term climate (Hedges et al., 1986; Richey et al., 1990, 2002; Mayorga et al., 2005; Bouchez et al., 2010, 2014; Ward et al., 2013, 2015; Sun et al., 2017)

In large river basins, spatial heterogeneity is a significant challenge to quantifying annual, basin-wide POC fluxes (Bouchez et al., 2011b; Galy et al., 2008; Lupker et al., 2011). The majority of knowledge on riverine particulate geochemistry and POC transport through the Amazon River mainstem has accrued through years of field measurements collected near the municipality of Óbidos in the State of Pará (Fig. 1a), the most downstream gaging station unaffected by seawater intrusion from the Atlantic Ocean (Kosuth et al., 2009; Moreira-Turcq et al., 2003; Richey et al., 1986). In the mainstem near Óbidos, which is about two kilometers wide

and over 60 meters deep during some seasons of the year, hydrodynamic sorting might cause larger grain-size sediments to settle faster and concentrate at deeper depths (Bouchez et al., 2011b; Curtis et al., 1979; Rouse, 1950) leading to compositional differences between deeper, coarser sediments and shallower, finer sediments (Bouchez et al., 2014; Bouchez et al., 2011a). In particular, depth-specific differences in total suspended sediment (TSS) concentrations in the mainstem cross-section can change five-fold (Bouchez et al., 2011a), implying that measurements traditionally based on surface TSS concentrations alone are susceptible to considerable error. For this reason, more recent Amazon POC export flux measurements have integrated across depths with sub-surface measurements (e.g., Bouchez et al. 2011b; Bouchez et al. 2014).

Potential depth-dependent differences in organic matter composition in the Amazon River have been explored less, but have implications for our understanding of the sources of POC that are eventually exported to the Atlantic Ocean. Here, we analyze particulate organic matter (POM) from two cross-sectional surveys at Óbidos during two stages of the river's hydrological cycle (i.e., rising and falling water levels), integrating measurements of the bulk POM pool with compound-specific lipid abundances and carbon stable isotope composition. While bulk metrics shed light on the predominant origins of organic matter in the river (Kim et al., 2012; Martinelli et al., 1994; Powell et al., 2012), lipid-specific measurements provide a nuanced understanding of specific carbon sources in the bulk pool, such as terrestrial vegetation and *in situ* primary production (e.g., Saliot et al. 2001; Häggi et al. 2016; Feakins et al. 2018). Our results expand understanding of the variability of POC composition in the narrow and deep mainstem of the Amazon River. To our knowledge, these data represent the highest resolution survey of POC within an Amazon mainstem cross-section.

Our study further compiles analyses of surface riverine POC samples collected from tributaries both upstream and downstream of our main study location (Óbidos). At this location on the mainstem, the Amazon River's particle composition integrates suspended sediments from most of the major tributaries of the drainage basin, particularly the Solimões and Madeira rivers, which join to form the Amazon upstream of Óbidos. Importantly, particle input from the Tapajós, Xingu, and Tocantins Rivers downstream can still alter the composition of POC that is ultimately exported to the Atlantic Ocean (Ward et al., 2015). Following prior studies that have attempted to sample river suspended sediments along transects, and understand the loss and

129 replacement of POC from the floodplain to the mouth (e.g., Hedges et al. 1986; Guyot et al.
130 1996; Kim et al. 2012; Ward et al. 2015; Häggi et al. 2016; Sun et al. 2017), our study endeavors
131 to contextualize the cross-sectional distribution of POC composition at Óbidos within a range of
132 new and previously published observations of POC both upstream and downstream.
133
134 **2 Methods**
135 *2.1 Overview of sampling expeditions*
136 The suspended sediments we discuss in this study were sampled during three expeditions
137 to the Amazon River Basin in June 2005, April 2014 and July 2014 (Table 1, Fig. 1a). The 2005
138 samples were collected from the mainstem at Óbidos, and at two upstream locations near the
139 Madeira River mouth to the Amazon River (~Foz Madeira) and near the Solimões River
140 connection to the mainstem (~Manacapuru). The reader may refer to Bouchez et al. (2011b) for
141 more description on the field collection and archival of these samples. The 2014 samples were
142 collected primarily at Óbidos. Sampling occurred once in the rainy season in March/April, and
143 once in the dry season, July 2014. In July 2014, suspended sediments were also retrieved from
144 the Tapajós River downstream from Óbidos.
145 In 2014, mainstem discharge at Óbidos varied by a factor of two between a minimum
146 during the dry season and a maximum during the rainy season (Fig. 1b). Continuous gauge
147 measurements near Óbidos (https://www.snirh.gov.br/hidroweb/serieshistoricas), conducted by
148 the Brazilian Agência Nacional de Águas, showed that in 2014, discharge peaked in May and
149 June at ~250,000 m^3/s (Fig. 1b). Thus, the two sampling months in 2014 reflect different river
150 stages, rising in April and falling in July, prior to and after peak discharge, respectively.
151 Each expedition served a unique purpose in this study. The two 2014 expeditions to
152 Óbidos provided the majority of samples we analyze in this study, as well as an opportunity to
153 quantify TSS and POC fluxes during two hydrological stages of the river, using a depth-
154 integrated method complementary to the prior expeditions (Bouchez et al., 2011b). The other
155 samples collected in 2005 and the one Tapajós River sample collected in 2014 allowed for an
156 extended comparison between Amazon River POC at Óbidos and POC from its most immediate
157 upstream and downstream tributaries.

158 Table 1. *Sample Locations and Times.*
159

River	Location	Latitude	Longitude	Date	Channel position	Sample depth	Temperature	Volume	Discharge	zR	TSS flux	POC flux
--	--	*°S*	*°W*	--	*km*	*m*	*°C*	-	*m3/s*	*unitless*	*kg/s*	*kg/s*
mainstem	Óbidos	1.937*	55.503*	8 June 2005	-	0	no data	>100 L	128,000	0.39	61,300	604
Madeira	Foz Madeira	3.456*	58.808*	6 June 2005	-	0	no data	>100 L	21,800	0.10	1,300	14
Solimões	Manacapuru	3.314*	60.554*	4 June 2005	-	0	no data	>100 L	124,700	0.09	17,400	168
mainstem	Óbidos	1.946	55.510	2 April 2014	0.32	35.49	25.9	~10 L	270,000	0.26	53,000	544
mainstem	Óbidos	1.946	55.510	2 April 2014	0.32	15.3	27.3	~10 L	270,000	0.26	53,000	544
mainstem	Óbidos	1.946	55.510	2 April 2014	0.32	2.1	no data	~10 L	270,000	0.26	53,000	544
mainstem	Óbidos	1.942	55.503	2 April 2014	1.1	49.1	no data	~10 L	270,000	0.26	53,000	544
mainstem	Óbidos	1.942	55.503	2 April 2014	1.1	30.15	27.5	~10 L	270,000	0.26	53,000	544
mainstem	Óbidos	1.942	55.503	2 April 2014	1.1	13.33	26.8	~10 L	270,000	0.26	53,000	544
mainstem	Óbidos	1.942	55.503	2 April 2014	1.1	2.7	26.4	~10 L	270,000	0.26	53,000	544
mainstem	Óbidos	1.938	55.496	2 April 2014	2.00	27.8	27.5	~10 L	270,000	0.26	53,000	544
mainstem	Óbidos	1.938	55.496	2 April 2014	2.00	10.4	26.1	~10 L	270,000	0.26	53,000	544
mainstem	Óbidos	1.938	55.496	2 April 2014	2.00	2.8	26.1	~10 L	270,000	0.26	53,000	544
mainstem	Óbidos	1.940	55.501	1 April 2014	-	0	28.0	>100 L	270,000	N/A	53,000	544
Tapajós	Tapajós	no data	no data	27 July 2014	-	0	no data	>100 L	no data	N/A	no data	no data
Tapajós	Tapajós	no data	no data	27 July 2014	-	bed	no data	N/A	no data	N/A	no data	no data
mainstem	Óbidos	1.946	55.509	28 July 2014	0.34	42.8	28.9	~10 L	249,000	0.34	48,000	369
mainstem	Óbidos	1.945	55.510	28 July 2014	0.34	20.6	no data	~10 L	249,000	0.34	48,000	369
mainstem	Óbidos	1.945	55.509	28 July 2014	0.34	3.5	no data	~10 L	249,000	0.34	48,000	369
mainstem	Óbidos	1.944	55.494	28 July 2014	1.6	54	28.9	~10 L	249,000	0.34	48,000	369
mainstem	Óbidos	1.942	55.497	28 July 2014	1.6	39.83	29	~10 L	249,000	0.34	48,000	369
mainstem	Óbidos	1.941	55.499	28 July 2014	1.6	30.4	28.9	~10 L	249,000	0.34	48,000	369
mainstem	Óbidos	1.941	55.499	28 July 2014	1.6	14.95	no data	~10 L	249,000	0.34	48,000	369

mainstem	Óbidos	1.939	55.501	28 July 2014	1.6	3.14	no data	~10 L	249,000	0.34	48,000	369
mainstem	Óbidos	1.933	55.497	28 July 2014	2.2	53.06	29	~10 L	249,000	0.34	48,000	369
mainstem	Óbidos	1.931	55.499	28 July 2014	2.2	29.83	no data	~10 L	249,000	0.34	48,000	369
mainstem	Óbidos	1.933	55.498	28 July 2014	2.2	3.33	no data	~10 L	249,000	0.34	48,000	369
mainstem	Óbidos	1.942	55.496	28 July 2014	-	0	29.2	>100 L	249,000	0.34	48,000	369
mainstem	Óbidos	no data	no data	28 July 2014	-	bed	no data	N/A	249,000	N/A	48,000	369
mainstem	Óbidos	no data	no data	28 July 2014	-	bed	no data	N/A	249,000	N/A	48,000	369
mainstem	Óbidos	no data	no data	28 July 2014	1	flood	no data	N/A	249,000	N/A	48,000	369

Note: Depth-specific samples at Óbidos were collected in three positions across the mainstem channel, referenced to the right bank across from Óbidos (Fig. 1). The 2005 data are taken from Bouchez et al. (2011b) and Bouchez et al. (2014). Discharge, total suspended solid (TSS) and particulate organic carbon (POC) fluxes, and water temperatures are provided when available. In the sample depth column, "bed"=bedload and "flood"=floodplain deposit.

* Latitude & longitude reflects one GPS coordinate for this sampling station and date

166 *2.2 Particle collection*

167 All suspended sediments were collected by filtering several large-volume (100-200 L)
168 samples of surface river water and a number of small-volume (~10 L) samples at specified
169 depths below surface. The exact volumes were calculated by weighing the water samples after
170 collection and converting mass to volume using the density of fresh water, ~1 kg/L. With the
171 exception of the 2005 samples, all water samples were filtered in pressurized Teflon-coated units
172 through 0.22 μm diameter pore size Millipore PES membrane filters within two days after
173 collection. Between collection and filtration, samples were either covered in a dark tarp or stored
174 in the shade to minimize exposure to sunlight. After filtration, the particles on the filters were
175 immediately frozen on board the ship. Although previous studies have highlighted the
176 compositional differences across particle size fractions in the Amazon River (Aufdenkampe et
177 al., 2007; Hedges et al., 1986, 1994), we have chosen to pool all particles above 0.22 μm in
178 diameter for analysis of the total riverine particle pool, following Bouchez et al. (2011b).

179 The large-volume samples were acquired at Óbidos (April 2014, July 2014 and June
180 2005), and each upstream/downstream tributary site using a bucket submerged a few tens of
181 centimeters below the surface. Each sampling location was roughly in the center of each river
182 channel. The 10 L samples were collected within three depth profiles at Óbidos in April and July
183 2014, using a depth-specific horizontal isokinetic sampler. Each profile, consisting of three to
184 five depths from 2-3 m to ~50 m, was located at a different position in the channel of the
185 mainstem between the right bank and the left bank closer to Óbidos (Fig. 1c, d, Table 1). The
186 depth-specific water sampler was equipped with a depth sensor to accurately record the
187 collection depths.

188 In July 2014, additional bedload samples from the Tapajós River and mainstem at Óbidos
189 were taken using a dredge sampler. One flood deposit sample from the right bank of the
190 mainstem, across from Óbidos, was also collected during this same expedition. Similar to the
191 water-column particle samples, these bedload and flood deposit samples were immediately
192 frozen following collection until analysis.

193 In the laboratory, each suspended sediment sample was re-suspended from the filters in
194 milli-Q water and freeze-dried, while bed samples and the floodplain deposit were directly
195 freeze-dried. All dried samples were sieved through a 2 mm mesh to remove any coarse
196 impurities such as rock fragments and leaf debris, and homogenized before subsequent analyses.

The homogenized quantities of suspended sediments were weighed to calculate suspended sediment concentrations (mg/L).

2.3 Flux calculations

During both sampling trips, on 3 April and 29 July 2014, water velocity profiles were measured across the mainstem channel using a *Sontek RiverSurveyor® M9* Acoustic Doppler Current Profiler (ADCP). The ADCP operated on a 1 MHz frequency, and was equipped with a 0.5 MHz vertical beam sensor for river depth measurements and an external GPS for compass heading, latitude and longitude tracking. The external GPS did not function over most of the transect in April, so an average offset from the external GPS was applied to correct the internal *Sontek* compass, which did provide continuous heading measurements. The *RiverSurveyor®* software integrated velocities measured through the instrument's transect and modeled within the "edge" regions between each end of the instrument transect and the nearest river bank to calculate a water discharge value through the river's cross-section.

The velocity cross-sections guided our choice of sample depths and locations for each depth profile (Fig. 1c, d, Table 1, Sect. 2.2) and enabled us to calculate suspended sediment fluxes across the mainstem. The ADCP measured three velocity components (E, N, U) down to 40 m depth. Horizontal velocities, V_{mag}, were calculated as the vector combination of the E (east) and N (north) components. Because 40 m was often shallower than the river bed and a further 10% of each velocity profile data was discarded prior to data export, the deepest measured velocities had to be extrapolated to the river bed, using the following relationship between horizontal velocity, V_{mag}, and vertical distance above river bed, z (Chen, 1989; Mueller et al., 2009):

$$V_{mag} = a_v z^{1/6} \quad (1)$$

The a_v values for each ADCP transect position were first extracted by fitting the measured V_{mag} profiles to Equation 1. Then, the extrapolated V_{mag} values for all depths between the deepest measured V_{mag} and the river bed were calculated using the fitted a_v values.

Suspended sediment concentration profiles (C_z) were modeled based on the assumption that the Amazon River mainstem was deep enough in April and July 2014 to allow for separation

of sediment grain size and density by depth. Following Bouchez et al. (2011b), who also reported hydrodynamic sorting in the Amazon mainstem, all depth-specific suspended sediment concentrations from each sampling month were fitted to a Rouse equation, which relates sediment concentration to river depth (Rouse, 1950):

$$\frac{C_z}{C_a} = \left(\frac{H-z}{z}\frac{a}{H-a}\right)^{z_R} \quad (2)$$

In this relationship, C_z is suspended sediment concentration at z, the vertical distance above the river bed, which has a depth of *H*. The constant *a* is the depth of the shallowest point measurement in the depth profile, C_a is the suspended sediment concentration at a, and z_R is the Rouse number. We used a nonlinear least-squares fit to calculate the Rouse number for April and July. The Rouse fits allowed us to model C_z across the entire mainstem cross-section by varying *H* from the ADCP data, but using constant C_a values, averaged across the surface-most measurement of the three channel positions in each sampling month.

We calculated suspended sediment fluxes at Óbidos during each sampling month by integrating the product of suspended sediment concentration (C_z, modeled by Equation 2) and water velocity (both measured and extrapolated V_{mag} values, according to Equation 1) across channel position and over river depth (Bouchez et al., 2011b):

$$\text{TSS flux} = \iint V_{mag} C_z \, dx \, dz \quad (3)$$

In Equation 3, *dx* values were calculated by projecting the distance of the boat track using ADCP transect coordinates (Fig. 1) against the azimuth of the mainstem at Óbidos.

2.4 Enzyme activity assays

Enzyme assays were conducted on suspended particles from the July 2014 Óbidos depth profiles to probe variations in heterotrophic activity in the Óbidos cross-section. Samples were analyzed using –AMC (7-amino-4-methylcoumarin) and –MUB (4-methylumbelliferone)-based fluorogenic substrate proxies (Mullen et al., 2018) (Table 2) and buffered with 100 mM carbonate buffer (pH=6.85). Assays were performed in triplicate for all samples and for one control, boiled to denature all enzymes, which served as a blank correction. Fluorescence was

measured three to four times during 4-hour sample and control incubations in 1 mL cuvettes at ambient temperature. Enzyme activities in each sample were inferred by the blank-subtracted substrate hydrolysis rates calculated from these four time points.

Table 2. *Substrates for Measuring Enzyme Activities in the Amazon River Mainstem, July 2014.*

Substrate	Abbreviation	Enzyme	Element
leucine-AMC	Leu-AMC	leucyl aminopeptidase	N
Phenylalanine-AMC	Phe-AMC	phenyalanyl aminopeptidase	N
Ala-Ala-Phe-AMC	AAF-AMC	chymotrypsin	N
MUB-beta-N-acetyl glucosamine	MUB-NAG	N-acetylglucosaminidase	N
MUB-cellobiose	MUB-cello	cellulase	C
MUB-beta glucose	MUB-beta-glu	beta-glucosidase	C
MUB-beta xylose	MUB-xyl	xylanase	C
MUB-PO4	MUB-PO4	phosphomonoesterase	P

Note: AMC is -amino-4-methylcoumarin and MUB is 4-methylumbelliferone.

2.5 Bulk particle composition

The distribution of grain sizes in the homogenized particle samples (Sect. 2.2) was analyzed using a Beckman Coulter Laser Diffraction Particle Size Analyzer (LS 13 320). Samples were sonicated for 10 seconds in tap water before loading into the detector. The LS 13 320 detects particles in the 0.4 μm to 2 mm size range, and reports mean and median grain size for each sample. The software additionally calculates the volumetric contribution of particle sizes throughout the distribution, as well as the d10, d50, and d90 diameters, which delineate the 10^{th}, 50^{th} and 90^{th} percentiles of the size distribution, respectively.

Bulk weight % organic carbon (%OC), weight % total nitrogen (%N), $\delta^{13}C$, and $\delta^{15}N$ in the homogenized suspended and bed sediments were analyzed using a *Fisons Instruments Carlo Erba 1108* elemental analyzer interfaced via a *Finnigan MAT Conflo II* to a *Delta-Plus* Stable Light isotope ratio mass spectrometer (IRMS). Prior to measuring % OC and $\delta^{13}C$, sub-samples were weighed, loaded in silver boats, fumigated in concentrated hydrochloric acid (12 N HCl) vapors for 72 hours at 60°C, and then dried in a desiccator at 60°C for 72 hours to remove the inorganic carbon in the sediment (Whiteside et al., 2011). One bedload sediment from Óbidos was analyzed after just 12-16 hours of acid fumigation. Weighed sub-samples were not

fumigated prior to measuring %N and $\delta^{15}N$. All analyses were conducted in triplicate. The results only report the average and standard deviation of the triplicate measurements.

For bulk radiocarbon composition, sub-fractions of selected sediment samples were similarly decarbonated via acid fumigation for 72 hours. After drying, the fumigated sample was sealed in an evacuated quartz tube with 2 g copper oxide, and baked at 850°C for 6 hours, which converted all the sample organic carbon to CO_2 gas (McNichol et al., 1995). The evolved CO_2 was then cryogenically purified under vacuum, graphitized by iron catalysis in pure H_2 gas at 450°C, and analyzed for its radiocarbon composition at the National Ocean Sciences Accelerator Mass Spectrometry (NOSAMS) facility at Woods Hole Oceanographic Institution (McNichol et al., 1992).

2.6 Compound-specific lipid analysis

Abundances of specific biomolecules provide higher-resolution details of organic matter composition. Straight-chain *n*-alkanes and fatty acids were quantified in each large-volume sample collected in 2005 and 2014, and in four depth-specific samples collected in 2014 (Table 1). Total lipids were extracted from sediment into 15-20 mL of 9:1 dichloromethane (DCM)/methanol at 100°C for 20 minutes using a Microwave Accelerated Reaction System (MARS, CEMS Corp.). The total lipid extracts were then saponified in 15 mL of 0.5 M potassium hydroxide (KOH) in wet methanol at 70°C for two hours. After adding 20 mL milli-Q water and 0.5 g of sodium chloride to the KOH solution, the basic lipids were extracted from the aqueous phase via five hexane rinses. The remaining KOH solution was acidified to pH~2 using 12 N HCl to isolate the acidic lipids in five rinses with 4:1 hexane/DCM.

Each basic and acidic lipid fraction was separated into five biomolecular classes on the basis of polarity. The concentrated lipid fractions were loaded onto aminopropyl silica gel columns and sequentially flushed with hexane (for *n*-alkanes), 4:1 hexane/DCM (for ketones), 9:1 DCM/acetone (for sterols, alcohols and other polar compounds), 2.6% oxalic acid in methanol (for fatty acids), and 1:1 DCM/methanol (for residual compounds). Both acidic and basic fraction-derived fatty acids were re-combined and methylated in 95:5 methanol:HCl with a known $\delta^{13}C$ value and ^{14}C composition for 12-16 hours at 70°C. The fatty acid methyl esters (FAMES) were isolated on an additional aminopropyl silica gel column after methylation. Prior to compound-specific isotope analysis, large-volume FAMES and *n*-alkanes were urea-adducted

315 in 40 mg/mL methanol urea solution as an additional purification step to separate the branched
316 compounds from straight-chain compounds. There was no need to further purify the four depth-
317 specific FAMES and *n*-alkane fractions that were selected for compound-specific isotope
318 analysis.
319 All compound abundances were measured using a flame ionization detector coupled to a
320 *Hewlett Packard 5890 Series II* Gas Chromatograph (GC-FID). Urea-adducted, combined acid
321 and base fractions of *n*-alkanes and FAMES were injected in high purity hexane. In addition, the
322 non-adducted fractions of FAMES and *n*-alkanes, as well as the other fractions of the post-
323 methylation FAMES columns were analyzed in the GC-FID. Any "residual" FAMES and *n*-
324 alkane quantities in these other fractions were added to the FAMES and *n*-alkane quantities from
325 the purified fractions, and are reported as such in Sections 3 and 4, all supplementary Tables and
326 Figures 4-6.
327 All GC-FID analyses were accompanied by a suite of standard *n*-alkanes and FAMES to
328 cross-reference sample peak retention times and quantify compound abundances by peak areas.
329 Some analyses were accompanied by just one standard injection at one known concentration,
330 while others were accompanied by injection of three different standard concentrations. When
331 three standard concentration chromatograms were available, standard curves were applied to
332 sample peak areas to estimate analyte mass (in nanograms). When analyses included just one
333 standard concentration, a response factor, equivalent to the average peak area/ng compound
334 across standard compounds, was used to convert sample peak area to mass.
335 The $\delta^{13}C$ values of specific FAMES and *n*-alkanes were measured using a *HP6890* gas
336 chromatograph fitted with a *Gerstel PTV* and interfaced via a *Finnigan MAT Conflo II* to a
337 *Delta-Plus* IRMS. When compound abundances were sufficient, $\delta^{13}C$ values were measured in
338 duplicate or triplicate, with only average and standard deviation values reported.
339
340 *2.7 Error analysis*
341 We equate the error of the average %OC, %N, bulk $\delta^{13}C$ and $\delta^{15}N$, and compound-
342 specific $\delta^{13}C$ to the standard deviation of triplicate analyses of each sample. Because the relative
343 errors in bulk F_m values were small, ranging from ~0.2%-0.5%, they are not reported in the
344 following sections. A conservative relative error of ±10% was used for lipid masses per

extraction, based on the relative standard deviation of standard compound peaks across GC-FID analyses. Errors were propagated for any metrics calculated from these values.

3 Data

3.1 Mainstem discharge in 2014

Maximum river depth of the Amazon River mainstem at Óbidos was 67-68 m in both April and July 2014, varying more by channel position than by season (Fig. 1). The *M9 RiverSurveyor*® ADCP logged >1400 velocity profiles from surface to riverbed in April and >1300 profiles in July. The average water velocity across the transect was 2.0 ± 0.6 m/s in April and 1.7 m/s ± 0.6 m/s in July. In both seasons, velocities tended to be highest (3-4 m/s) in the middle of the cross-section, where depths exceeded 40 m. Velocities near the river bed were generally slower, less than 1.5 m/s. Total calculated discharge (Sect. 2.3) at Óbidos decreased slightly between sampling months, ranging from 270,000 m^3/s in April and 249,000 m^3/s in July (Table 1). While our July value was consistent with measurements from the Brazilian Agencia Nacional de Aguas (Fig. 1b), our instantaneous April value overestimated discharge at Óbidos by ~18%.

3.2 TSS concentrations and fluxes in 2014

Total suspended sediment concentrations ([TSS]) throughout the main-stem cross-section at Óbidos varied from 55.5 to 318.5 mg/L in April 2014 (Fig. 2, Table 3), within the range of all suspended sediment concentrations analyzed at Óbidos in 2005 (Bouchez et al., 2011a). July values were broader, ranging from 16.4 to 741.4 mg/L. Concentrations were highest in the deepest samples near the right bank (i.e., across from the municipality of Óbidos) in both April and July 2014. Positioned inside of a bend in the Amazon mainstem, a greater abundance of particles accumulates in river waters here, leading to significantly higher TSS concentrations (i.e., greater than mean + 1 S.D. of all other depth-specific [TSS] values). In July, this deep sample has the highest C/N value of all depth-specific samples from the same sampling period, potentially bearing the signature of re-suspended organic matter deposits from the adjacent river bank, which has a higher C/N value compared to the other April/July suspended sediments.

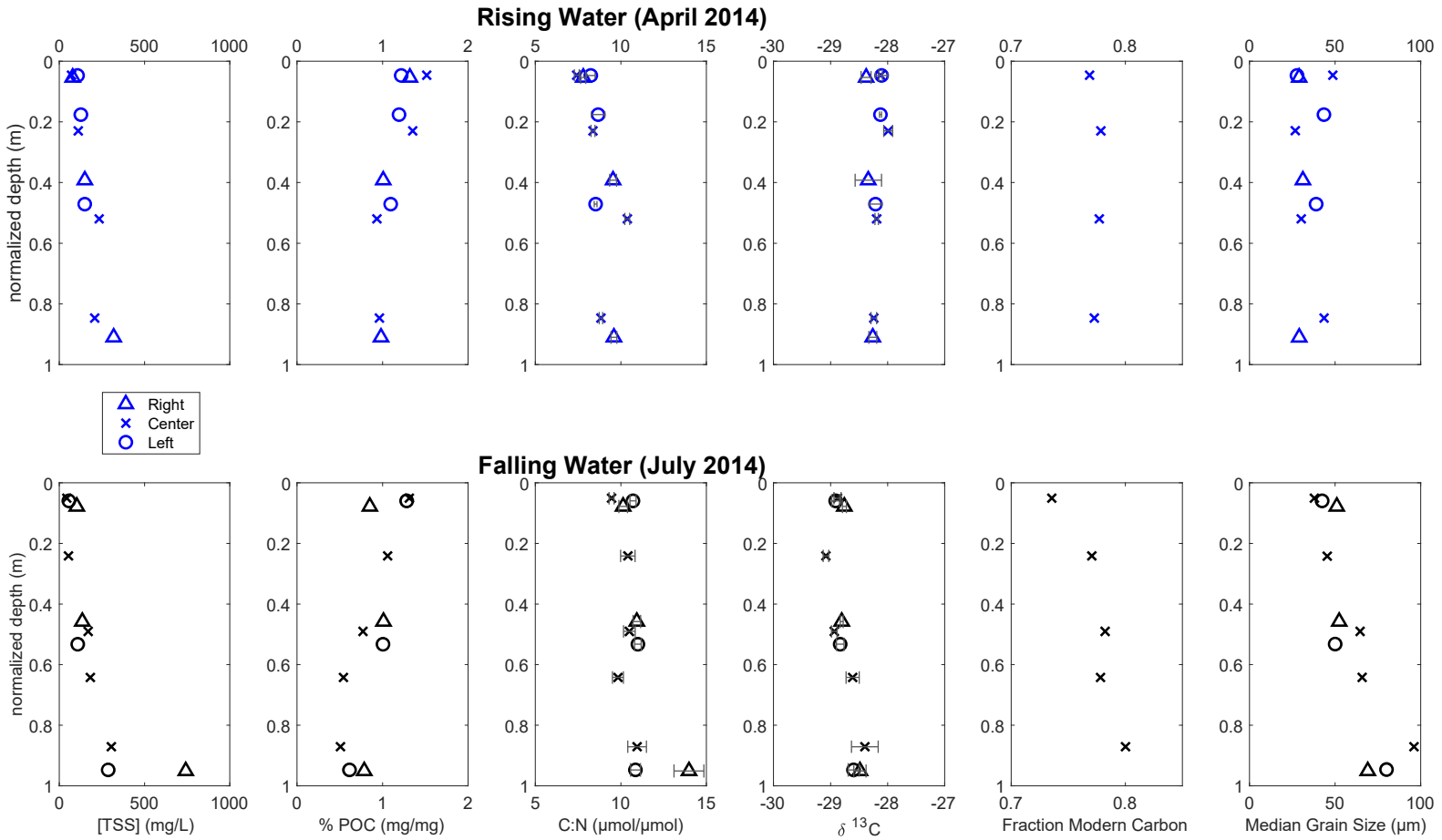

Figure 2. Profiles of TSS concentration, organic matter composition, and median grain size (d50) at Óbidos in April (blue) and July (black) 2014. Data from profiles near the right bank (triangles), left bank (circles) and river center (crosses) are separate. All y-axes are normalized to the river depth at the channel position of each profile. The errors in %POC, %PN and fraction modern are relatively small and therefore not plotted. $\delta^{13}C$ values are expressed in units of ‰.

382 Table 3. *Total Suspended Sediment Concentration, Organic Matter Composition and Grain Size of 2005 and 2014 Samples.*

383

Location	**Depth**	**Channel position**	**[TSS]**	**%POC**	**%PN**	**C/N**	**$\delta^{13}C$**	**Fraction modern**	**Grain-mean**	**Grain-d50**	**Grain-d10**	**Grain-d90**
--	*m*	*km*	*mg/L*	*mg/mg*	*%*	*µmol/ µmol*	*‰*	*unitless*	*µm*	*µm*	*µm*	*µm*
mainstem*	0	-	no data	0.85 ± 0.01	0.14 ± 0.005	7.3 ± 0.5	-28.5 ± 0.05	0.71	no data	no data	no data	no data
Solimões*	0	-	no data	1.12 ± 0.06	0.17 ± 0.003	7.9 ± 1.8	-27.0 ± 0.05	0.72	no data	no data	no data	no data
Madeira*	0	-	no data	0.49 ± 0.01	0.08 ± 0.0004	7.2 ± 1.9	-27.7 ± 0.3	0.67	no data	no data	no data	no data
mainstem	0	-	55	1.37 ± 0.01	0.19 ± 0.004	8.5 ± 0.2	-28.1 ± 0.06	0.72	no data	no data	no data	no data
mainstem	35.49	0.32	319	0.98 ± 0.02	0.12 ± 0.001	9.6 ± 0.2	-28.3 ± 0.07	no data	44	29	4	109
mainstem	15.3	0.32	150	1.01 ± 0.02	0.12 ± 0.001	9.5 ± 0.2	-28.3 ± 0.2	no data	48	31	5	121
mainstem	2.1	0.32	79	1.32 ± 0.02	0.20 ± 0.001	7.8 ± 0.1	-28.4 ± 0.09	no data	50	29	4	131
mainstem	49.1	1.1	208	0.96 ± 0.01	0.13 ± 0.001	8.8 ± 0.1	-28.2 ± 0.05	0.77	63	44	6	153
mainstem	30.15	1.1	233	0.93 ± 0.01	0.11 ± 0.001	10 ± 0.1	-28.2 ± 0.03	0.78	48	30	5	119
mainstem	13.33	1.1	111	1.35 ± 0.01	0.19 ± 0.002	8.4 ± 0.1	-28.0 ± 0.08	0.78	43	27	4	106
mainstem	2.7	1.1	72	1.52 ± 0.01	0.24 ± 0.004	7.4 ± 0.1	-28.1 ± 0.03	0.77	70	49	4	171
mainstem	27.8	2.00	149	1.09 ± 0.01	0.15 ± 0.001	8.5 ± 0.1	-28.2 ± 0.1	no data	61	39	5	154
mainstem	10.4	2.00	126	1.19 ± 0.05	0.16 ± 0.003	8.7 ± 0.4	-28.1 ± 0.02	no data	60	43	6	142
mainstem	2.8	2.00	107	1.22 ± 0.03	0.17 ± 0.002	8.2 ± 0.3	-28.1 ± 0.1	no data	44	28	4	110
Tapajós	bed	-	N/A	0.14 ± 0.002	0.017 ± 0.0003	10 ± 0.3	-29.4 ± 0.2	1.02	no data	no data	no data	no data
Tapajós	0	-	0.52	15.71 ± 0.13	2.69 ± 0.005	6.8 ± 0.1	-31.0 ± 0.1	0.89	no data	no data	no data	no data
mainstem	0	-	16	1.80 ± 0.02	0.23 ± 0.003	9.0 ± 0.1	-29.1 ± 0.06	0.77	no data	no data	no data	no data
mainstem	42.8	0.34	741	0.79 ± 0.04	0.07 ± 0.002	14 ± 0.9	-28.5 ± 0.1	no data	80	69	11	165
mainstem	20.6	0.34	135	1.01 ± 0.003	0.11 ± 0.002	11 ± 0.2	-28.8 ± 0.03	no data	71	52	9	163
mainstem	3.5	0.34	103	0.85 ± 0.02	0.10 ± 0.001	10 ± 0.3	-28.8 ± 0.03	no data	66	51	8	146
mainstem	54	1.6	305	0.51 ± 0.02	0.054 ± 0.001	11 ± 0.5	-28.4 ± 0.2	0.80	106	96	15	212
mainstem	39.83	1.6	182	0.54 ± 0.01	0.064 ± 0.002	9.8 ± 0.3	-28.6 ± 0.1	0.78	80	66	9	176

mainstem	30.4	1.6	169	0.77 ± 0.02	0.086 ± 0.001	11 ± 0.3	-28.9 ± 0.05	0.78	77	65	9	168
mainstem	14.95	1.6	53	1.06 ± 0.02	0.12 ± 0.004	10 ± 0.4	-29.1 ± 0.05	0.77	60	45	7	139
mainstem	3.14	1.6	44	1.31 ± 0.02	0.16 ± 0.002	9.5 ± 0.2	-28.9 ± 0.06	0.74	55	38	6	133
mainstem	53.06	2.2	286	0.61 ± 0.01	0.066 ± 0.001	11 ± 0.3	-28.6 ± 0.1	no data	93	80	13	194
mainstem	29.83	2.2	108	1.00 ± 0.01	0.11 ± 0.001	11 ± 0.2	-28.8 ± 0.07	no data	71	50	8	171
mainstem	3.33	2.2	56	1.28 ± 0.02	0.14 ± 0.0003	11 ± 0.2	-28.9 ± 0.07	no data	62	42	7	153
mainstem	flood	0	N/A	0.50 ± 0.03	0.048± 0.001	12 ± 0.9	-28.1 ± 0.08	no data	no data	no data	no data	no data
mainstem	bed	0	N/A	0.064± 0.002	0.0093±0.0004	8.0 ± 0.5	-26.6 ± 0.09	0.60	no data	no data	no data	no data
mainstem	bed	0	N/A	0.022± 0.001	BDL	no data	-26.9 ± 0.02	0.87	no data	no data	no data	no data

Note: Channel position for depth-specific samples at Óbidos are referenced to the right bank across from Óbidos (Fig. 1). Errors for C/N and $\delta^{13}C$ are reported. Relative errors of depth-specific F_m values are < 1%, and are not reported.

* 2005 sample (refer to Table 1 for specific sampling dates).

BDL= below detection limit.

"bed"=bedload.; "flood"=floodplain deposit.

Total suspended sediment concentrations increased with depth in all profiles at Óbidos (Fig. 2, Table 3). Other than in the right bank profiles in April, mean, median/d50, d10, and d90 grain size diameters generally increased with depth and [TSS], providing clear evidence for hydrodynamic sorting of sediment in the cross-section (Bouchez et al., 2011b; Rouse, 1950). All 10 L [TSS] values were fitted to the Rouse equation (C_z in Equation 2). We chose to combine profiles within each sampling month rather than calculate one Rouse number per channel position profile per month, following the reasoning that the errors from fitting individual, instantaneous profiles in a given depth profile could be offset by the spatial heterogeneity of three depth profiles spanning the cross-section (Bouchez et al., 2011b). The reference height above the river bed, z_a, varied from 36.9 m to 56.2 m in April and from 41.5 to 58.9 m in July. The suspended sediment concentration at z_a, C_a, varied from 71.6 to 106.8 mg/L in April and from 43.9 to 102.7 mg/L in July. These TSS concentration fits yielded a Rouse numbers of 0.26 and 0.34, respectively, in April and July (Table 1). The modeled concentration profiles fit the data well, suggesting that the Rousean description of hydrodynamic sorting adequately explains our observations (Fig. 3).

The integrated product of [TSS] and water velocity within each cross-section yielded instantaneous suspended sediment fluxes of ~53,000 kg/s in April and ~48,000 kg/s in July (Equation 3). We note that while these values do not incorporate water discharge and sediment concentrations within the cross-sectional area between each river bank and the ends of the ADCP transects (i.e., the "edge" discharge values calculated by the RiverSurveyor® software, as described in Sect. 2.3), discharge in these "edge" sections of the transect represents less than 1% of total discharge at the mainstem.

3.3 Bulk POC composition

The weight % organic carbon (%OC) within depth-specific sediments at Óbidos ranged from 0.51 - 1.52% and decreased with depth in all profiles across channel positions and seasons (Fig. 2, Table 3). At the same time, particulate organic carbon concentrations ([POC]), which ranged from 0.6 - 5.9 mg/L, increased with depth, as TSS concentrations increased. Weight % nitrogen (%N) values in suspended sediments ranged from 0.05 - 0.24% and also decreased with depth. Molar C/N ratios exhibited a large range from 7.4 to 14.1, and tended to increase with depth in all profiles. Even though [TSS], %OC, and [POC] varied within profiles at Óbidos, the

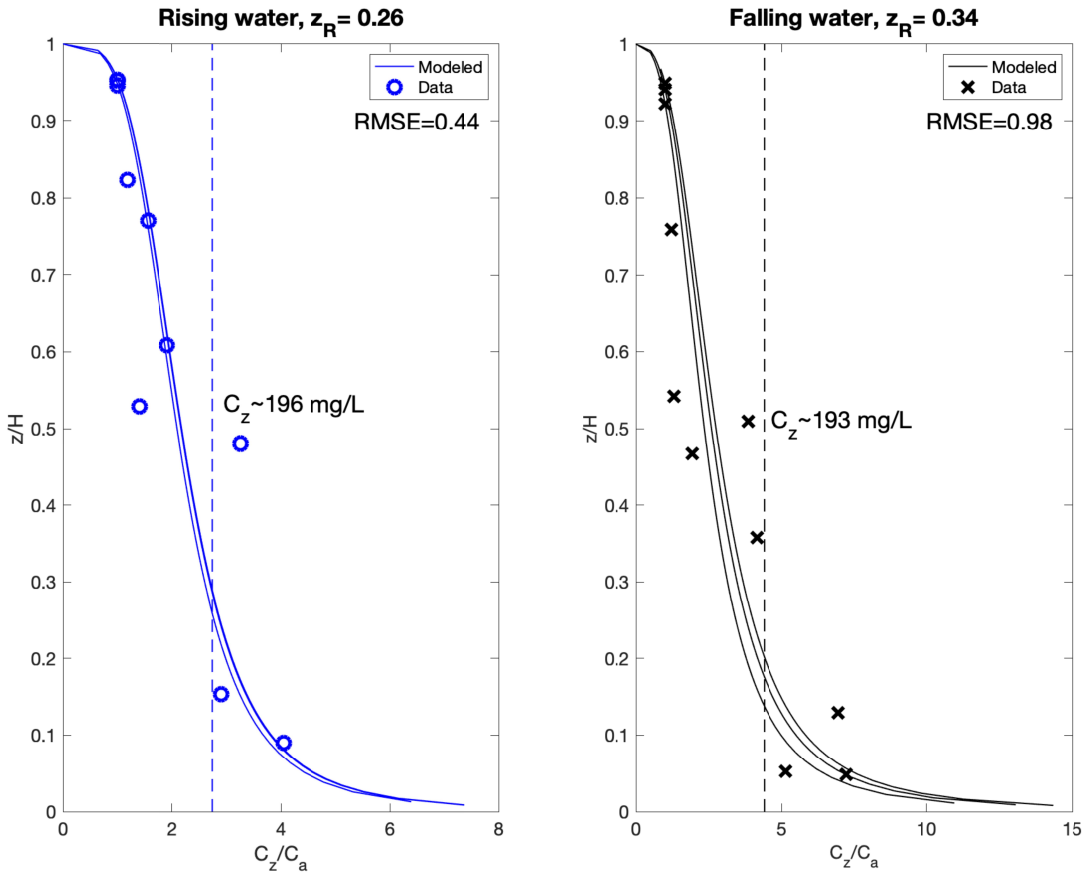

Figure 3. Fits of all depth-specific TSS concentration (C_z) profiles measured at Óbidos in 2014 to the Rouse Equation (Equation 2; Bouchez et al., 2011; Rouse 1950). Variable *z* is the height above the river bed *H* of each profile, and C_a is the surface-most measured C_z value of each profile. The vertical lines corresponding to C_z ~ 196 mg/L and 193 mg/L are the sediment concentrations needed to compute equivalent sediment fluxes based on sampling at a single (50%) depth.

isotopic composition of organic carbon in the sediments did not vary significantly with depth. $\delta^{13}C$ values ranged from -29.1‰ to -28.0‰ across all profiles and seasons, while $\delta^{15}N$ values ranged from 3.1‰ to 4.3‰. The range in fraction modern (F_m) values was also relatively small (0.74 - 0.80), corresponding to a radiocarbon age span of 680 years (1790 to 2470 years).

The composition of POC and particulate nitrogen in all mainstem surface samples collected in 2005 and 2014 was similar to the POC composition of the depth-specific samples from 2014. The only difference was that the POC in these surface samples was consistently older, with F_m values as low as 0.71 (2,760 years before present), than the POC analyzed at

specific depths. Surface suspended sediment concentrations in the Solimões and Madeira rivers, collected in 2005, were also similar to the range observed at Óbidos (Bouchez et al., 2011b). The % OC in these sediments ranged from 0.49% in the Madeira River to 1.12% in the Solimões River (Table 3). Weight %N ranged from 0.08% in the Madeira River to 0.17% in the Solimões River. Stable and radiocarbon measurements of POC in the Solimões and Madeira River sediments were slightly more ^{13}C-enriched and older than the Óbidos depth-specific samples. The Tapajós River had the most compositionally distinct suspended sediments of the data set. Surface suspended sediment concentrations in July 2014 were much lower than observed at any other river, only 0.52 mg/L. But, % OC in these sediments was the highest measured, 15.7%. Weight %N was also high, 2.69%. The F_m value was 0.89 (955 years before present), corresponding to a younger ^{14}C age than any of the values measured at Óbidos.

The weight %OC and %N in the three bed sediment samples from near the left bank of Óbidos, the right bank of Óbidos, and the Tapajós River were lower than corresponding values in all suspended sediment samples, ranging from 0.022% to 0.14% organic carbon and from 0.0027% to 0.017% nitrogen, consistent with other bedload observations in the basin (Bouchez et al., 2014) (Table 3). The $\delta^{13}C$ composition of bed samples at Óbidos and in the Tapajós River were consistently more ^{13}C-enriched (by ~1-2 ‰) than POC in suspended sediments in their respective rivers. While radiocarbon ages in the Óbidos bed samples ranged from F_m 0.60 (4,090 years before present) to 0.87 (1,100 years before present), we neglect the higher F_m value (0.87) on the basis of specimen contamination (e.g., fresher plant litter debris), as bed samples with such low %OC are typically older across the Amazon River Basin (Bouchez et al., 2010). The Tapajós bed sample was modern (F_m >1.0), younger than POC in the Tapajós suspended sediment. Values of %OC and %N of right bank flood deposit near the Óbidos cross-section were more similar to the range in depth-specific sediments, 0.50% and 0.048%, respectively. The stable isotope composition of the flood deposit was closer to the range observed across depth-specific suspended sediment samples, as well.

3.4 Lipid abundances and isotope composition

Measurements of leaf wax compounds provide a useful tool for tracing POC sources in complex mixtures like riverine sediments. Alongside our other analyses, these lipid abundances and carbon stable isotopes enable a more nuanced understanding of the organic matter pools that

contribute to bulk POC among different sampling seasons and tributary locations. Total lipids were extracted from all large-volume suspended sediment samples from the surface of the Amazon River mainstem (June 2005, April 2014 and July 2014), the Tapajós River (July 2014), the Solimões River (June 2005) and the Madeira River (June 2005), as well as from four depth-specific samples from the two 2014 Óbidos center profiles (Table 1). Compound-specific $\delta^{13}C$ values were not resolved for the April 2.7 m sample because the total lipid extract was too small. Compound-specific $\delta^{13}C$ values were also not measured in *n*-alkanes in the tributary samples.

Abundances of straight-chain *n*-alkanes in Óbidos samples were quantified for sixteen carbon chain lengths from 19 (C_{19}) to 35 (C_{35}), and ranged from 0.001 to 0.4 ng/μg of total POC (Table S1, Fig. 4a, 5c, e). Generally, POC-normalized compound abundances at Óbidos were greater at the surface than abundances measured deeper in the water column. The distribution of abundances above chain lengths C_{23} displayed an odd-over-even carbon chain length predominance in all samples, characteristic of terrestrial vegetation (Eglinton & Hamilton, 1963) (Fig. 5c, e). Average chain lengths (ACL) for *n*-alkanes (Equation 4a, Fig. 4c) spanned a small range from 29.6 to 30.1, decreasing slightly with depth.

$$\mathrm{ACL_{n-alkane}} = \frac{25[C_{25}]+27[C_{27}]+29[C_{29}]+31[C_{31}]+33[C_{33}]+35[C_{35}]}{[C_{25}]+[C_{27}]+[C_{29}]+[C_{31}]+[C_{33}]+[C_{35}]} \quad (4a)$$

$$\mathrm{ACL_{fatty\ acid}} = \frac{24[C_{24}]+26[C_{26}]+28[C_{28}]+30[C_{30}]+32[C_{32}]+34[C_{34}]}{[C_{24}]+[C_{26}]+[C_{28}]+[C_{30}]+[C_{32}]+[C_{34}]} \quad (4b)$$

By comparison, stable isotope values of odd chain-length *n*-alkanes spanned a larger range across months and depths than all $\delta^{13}C$ values measured in bulk POC from the Óbidos depth profiles, ranging from -37.3‰ to -28.3‰ (Fig. 4b, Table S1). Generally, lipids at the surface were more ^{13}C-enriched than lipids at deeper depths.

Relative abundances of straight chain *n*-alkanes in surface suspended sediments of the Solimões River were similar to relative abundances observed in the Óbidos samples (Fig. 5a), while Madeira River *n*-alkanes abundances were higher than both Óbidos and Solimões River samples, particularly for chain lengths 28-33. While *n*-alkanes from the Solimões River exhibited

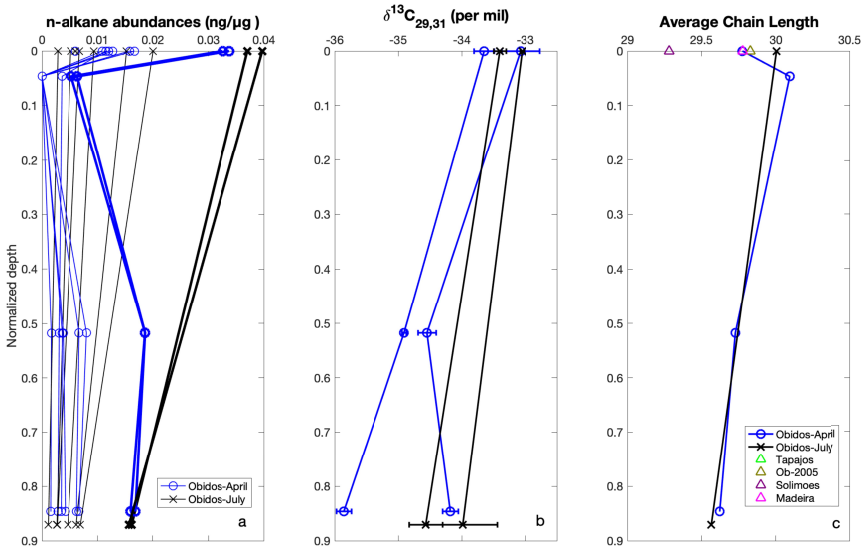

Figure 4. Depth profiles of *n*-alkane (a) abundances (ng/µg total particulate organic carbon), (b) $\delta^{13}C$ values (‰) and (c) average chain lengths (ACL) measured in Óbidos center profiles in April 2014 (blue) and July 2014 (black). Additional ACL values for surface samples at Óbidos in 2005 and different river tributaries are plotted, as well. Different lines in (a)-(b) plot values for a different chain length between 19 and 35. The thicker width lines in (a) plot chain lengths 29 and 31 only, highlighting the highest abundance *n*-alkanes.

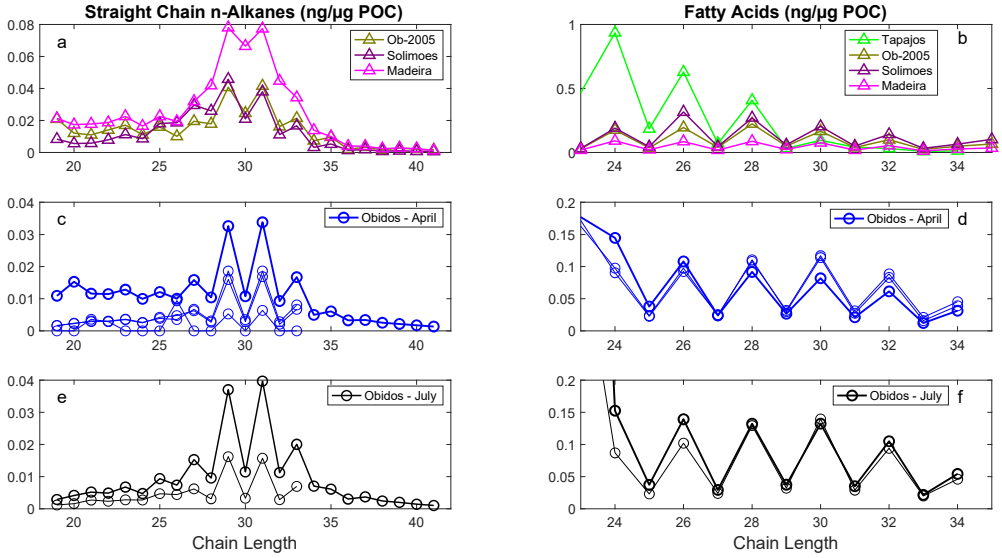

Figure 5. Abundances of (a, c, e) straight chain *n*-alkanes and (b, d, f) fatty acids measured in the Amazon River mainstem and tributaries over a range of longer chain lengths. Each line in the Óbidos April and July panels plots data from a different depth of the center profile, with the boldest line indicating data from the surface large-volume sample.

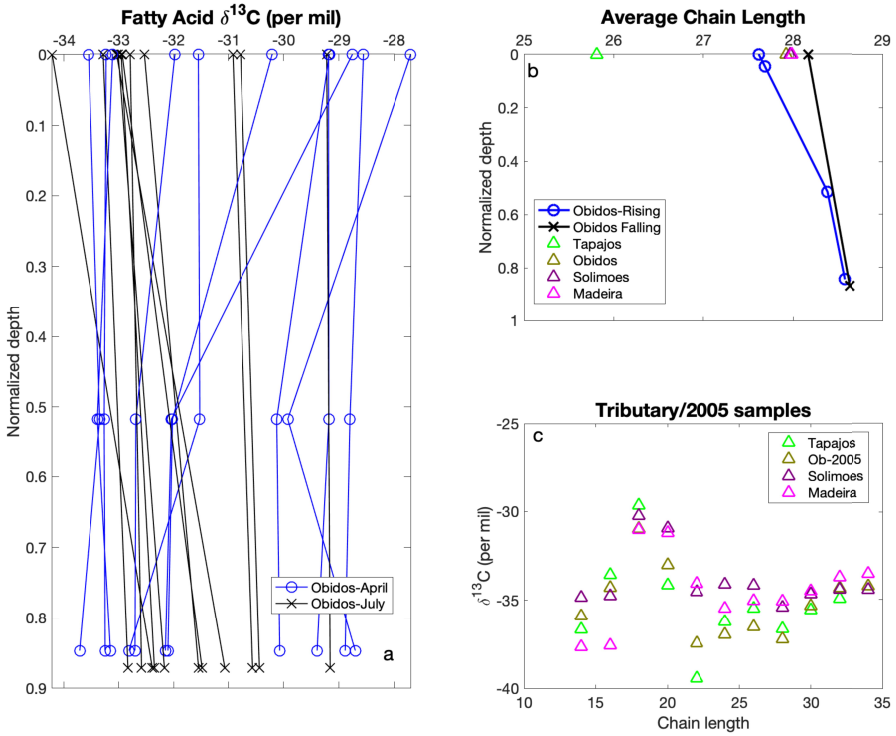

Figure 6. Profiles of fatty acid (a) $\delta^{13}C$ values (‰) and (b) average chain lengths (ACL) measured in mainstem samples collected at Óbidos in April (blue) and July (black) 2014. Each line in (a) plots values for a different chain length from 14 to 34, all showing little trends with depth. Additional ACL values are plotted for the surface samples taken from the Tapajós, Solimões and Madeira Rivers, and from the mainstem in 2005. Panel (c) plots fatty acid $\delta^{13}C$ values in these tributary and mainstem samples over a range of chain lengths.

odd-over-even predominance, as observed in the mainstem, the odd-over-even predominance in the *n*-alkanes from the Madeira River was weaker. Surprisingly, average chain lengths in all Óbidos and Madeira River samples were similar, while ACL values for the Solimões River sample were lower, 29.3 (Fig. 4c).

Abundances of saturated straight-chain fatty acids (C_{14}-C_{34}) measured at Óbidos ranged from 0.008 to 4.0 ng/µg POC (Fig. 5d, f, Table S2). In most samples, the most abundant compounds were C_{16} and C_{18} (0.18 – 4.0 ng/µg POC). At chain lengths above 22, the abundances exhibited even-over-odd predominance in all samples, reflecting an important contribution from terrestrial vegetation. Differences in relative fatty acid abundances at different sampling months

528 and across depths were negligible, though notable spillage of the large-volume surface sample
529 collected in July could have depressed abundances quantified by the FID. Average chain lengths
530 of fatty acids (Equation 4b, Fig. 6b) did increase with depth from 27.6 near the surface to 28.6 at
531 49 m in April 2014, and to a lesser extent from 28.2 near the surface to 28.6 at 54 m in July
532 2014. The stable carbon isotope composition of even chain-length fatty acids across the depth-
533 specific samples spanned a greater range than bulk $\delta^{13}C$ values in the same samples, from -
534 37.5‰ to -27.7‰ (Fig. 6a).
535 Straight-chain fatty acids were also quantified in surface suspended sediment samples
536 from the Tapajós, Solimões and Madeira rivers. The upstream tributary samples displayed strong
537 even-over-odd predominance among the higher chain-length fatty acids (Fig. 5b). Fatty acid
538 abundances and ACL values generally exhibited a similar range to the Óbidos samples (Table
539 S2, Figs. 5, 6b). Only the Tapajós River sample showed very elevated concentrations of C_{14}, C_{16}
540 and C_{18} that were up to ~100 times higher than the abundances of these fatty acids across all
541 other 2014 and 2005 samples, and the lowest ACL calculated in the data set (25.8). Compound
542 abundances from chain lengths 24 to 28 in the Tapajós River were also significantly elevated
543 relative to Óbidos, and Solimões and Madeira River samples. By contrast, differences in $\delta^{13}C$
544 values among Tapajos and other river samples were smaller. Even though the bulk POC from the
545 Tapajós River is relatively ^{13}C-depleted, only $\delta^{13}C$ values of fatty acid chain length 22 were
546 lower (e,g, $\delta^{13}C_{C22}$ = -39.4‰) than values at Óbidos and other tributaries (Fig. 6c).
547
548 *3.5 Enzyme activities*
549 Activities of eight extracellular enzymes measured at various depths within the Óbidos
550 cross-section in July 2014 ranged from 0 to 0.09 μmol/L-hr (Table S3, Fig. 7). Values generally
551 did not vary with depth or channel position. Activities of the N- and P-yielding enzymes (i.e.,
552 leucyl aminopeptidase, phenylalanyl aminopeptidase, and phosphomonoesterase) (Table 2),
553 exceeded activities of the C-yielding enzymes (i.e., cellulase, beta-glucosidase and xylanase)
554 throughout profiles.
555

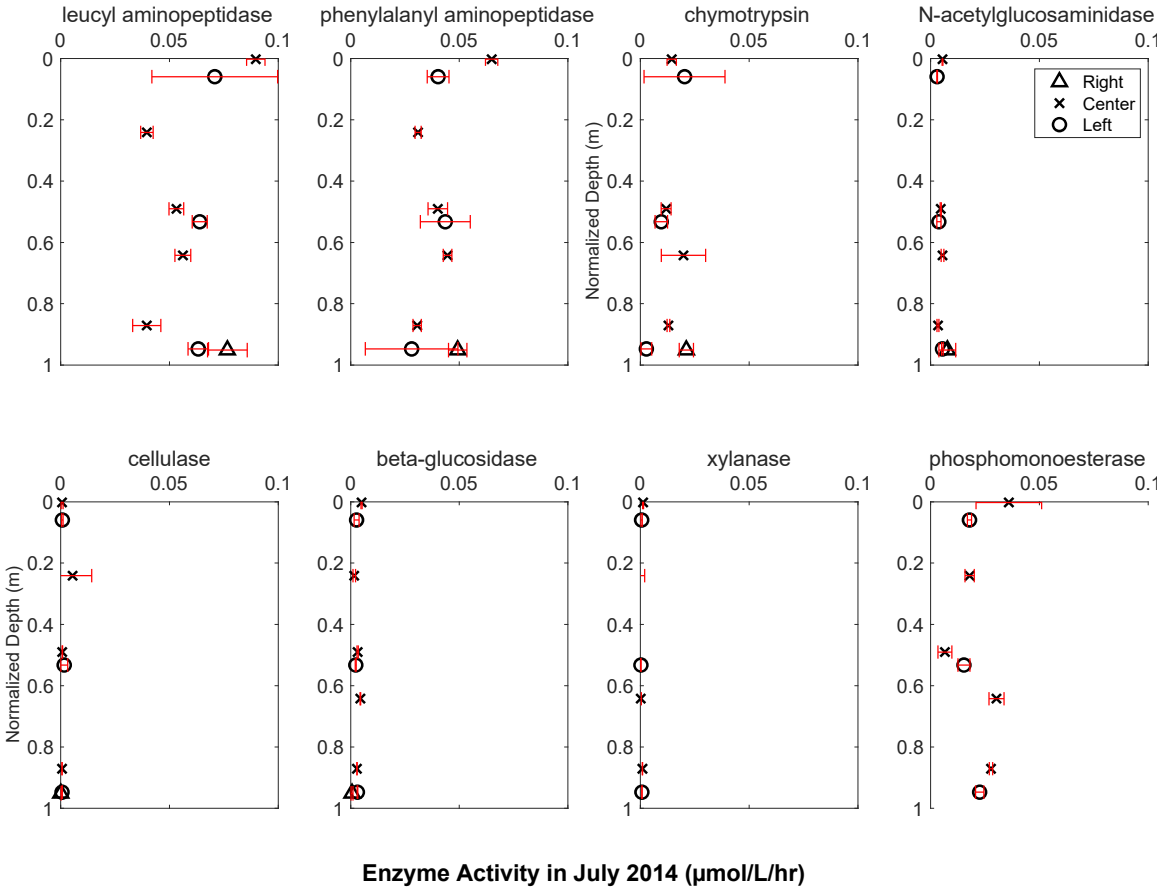

Figure 7. Activities of eight enzymes measured within the Óbidos cross-section in July 2014.

4 Discussion of results

The current study offers a cross-sectional survey of suspended particulate organic matter (POM) composition from the mainstem of the Amazon River during two stages of the river's annual hydrological cycle, 1-2 months before and after peak discharge. It is important to note that in the following analyses, from the total organic pool to compound-specific biomarkers, measurements represent a mixture of numerous carbon sources with diverse origins and degradation histories. The purpose of the current study is to interpret the predominant sources of organic matter that drive the composition of POC exported through the river cross-section.

4.1 TSS and POC flux at Óbidos

Increasing TSS concentrations with depth in all profiles compiled at Óbidos in April and July 2014 are indicative of hydrodynamic sorting (Rouse, 1950), and consistent with prior depth

profiles of the same size-fraction of sediments compiled by (Bouchez et al., 2011b) across the central Amazon River Basin (Figs. 2, 3). This is supported by even lower TSS concentrations in the surface large-volume samples (<1 m depth) (Table 3). Despite the lack of change in river discharge between April and July 2014, z_R values increased significantly, by 0.08 units from 0.26 to 0.34. The Rouse numbers that we report are similar in magnitude and temporal variation to the numbers estimated from profiles at Óbidos in March 2006 ($z_R = 0.24$) and June 2005 ($z_R = 0.39$) (Bouchez et al., 2011b).

Consistent increases in grain sizes with depth in July 2014 sediment profiles relative to April 2014 profiles (Student's t-test, $p<0.05$) could have enhanced the depth gradient in July sediment concentrations, leading to higher z_R values. This is consistent with a Ganga River study (Lupker et al. 2011), which partitioned and modeled Rouse profiles of suspended sediment concentrations by grain size, reporting higher z_R values for larger grain size profiles. Of the three major tributaries upstream of Óbidos, variations in the sediment-rich Solimões and Madeira Rivers contribute disproportionately to seasonal variations in sediment grain size in the mainstem, relative to the sediment-deplete Negro River (Kim et al., 2012). Although we do not have 2014 grain size data from these upstream tributaries, Bouchez et al. (2011) reported higher median grain diameters in the Solimões River relative to the Madeira River. Therefore, a higher relative discharge from the sediment-rich Solimões River in July, as was recorded by the Agência Nacional de Águas, would result in a larger gradient in [TSS] between river surface and river bed in July.

Overall, our TSS flux estimates (53,000 kg/s in April and 48,000 kg/s in July) are similar in magnitude, though less variable, to fluxes estimated by Bouchez et al. (2011b) in June 2005 and March 2006 (61,300 kg/s and 39,700 kg/s, respectively) (Table 1). They generally diverge from studies that estimate flux by multiplying discharge by TSS concentration at a single depth. For example, our fluxes are more than five times greater than surface-based fluxes calculated by Kim et al. (2012) during two expeditions to Óbidos in 2005 and 2009 (4-8 tons/second or 3600-7300 kg/s). Computing sediment fluxes equivalent to ours as the product $discharge \times [TSS]$ from a single depth requires TSS concentrations of 196 mg/L in April and 193 mg/L in July, much greater than surface values reported in Kim et al. (2012). Interestingly, other studies at Óbidos have focused on sampling TSS at the midpoint depth rather than at the river surface (Ward et al., 2015). As Fig. 3 illustrates, these target concentrations are greater than our modeled

603 Rousean TSS values at their midpoint depths, though some of our discrete midpoint samples are
604 close to 196 mg/L and 193 mg/L. Importantly, these juxtapositions are incomplete in that both
605 Kim et al. and Ward et al. sampled particles in different years and within different pore size
606 intervals, >0.7 μm and 0.45- 297 μm, respectively, compared to >0.2 μm in this study.
607 Nonetheless, they highlight the necessity and impact of accounting for cross-sectional variation
608 in [TSS] when calculating TSS fluxes out of the river cross-section.
609 Particulate organic carbon concentrations increased with depth alongside TSS. We
610 calculated POC fluxes during each sampling month by linearly regressing [POC] against [TSS]
611 (Equation 5), using a Type II regression function in Matlab. This yielded a slope (mg [TSS]/mg
612 [POC]) and intercept (mg/L [POC]) which can then be substituted into the Rouse-modeled C_z in
613 Equation 2:
614 $$[\mathrm{POC}] = \mathrm{m}[\mathrm{TSS}] + \mathrm{b} \quad (5)$$
615
616 In this equation, *m* is the slope of the linear relationship (0.0079 mg POC/mg TSS in April and
617 0.0072 mg POC/mg TSS in July) while *b* is the intercept (0.46 mg POC in April and 0.075 mg
618 POC in July). The integrated POC flux in April 2014 was 544 kg/s, while the integrated POC
619 flux in July 2014 was 369 kg/s **(**Table 1). This difference can be explained by a significant
620 decrease in the average %OC in depth-specific suspended sediments from 1.16 ± 0.2% (mean ±
621 1 S.D.) in April to 0.88 ± 0.27% in July (Student's t-test, $p<0.05$). Again, these fluxes are similar
622 to those reported in (Bouchez et al., 2014), and ~35-240% higher than those reported by Kim et
623 al. (2012) during high water. Scaling 544 kg/s or 369 kg/s to one year results in a flux of ~12-17
624 Tg/year, which is similar to earlier flux estimates of 14 Tg/year by (Richey et al., 1990),
625 who deployed a depth-integrated sampler to measure POC concentrations in fine (<63 μm) and
626 coarse (>63 μm) particles (Richey et al., 1986). Likely, our flux range overestimates the annual
627 POC flux because our April and July 2014 values represent the high discharge period only.
628 Moreira-Turcq et al. (2003) showed that fluxes could be much lower at lower discharge periods,
629 and reported annual average POC fluxes of 5.8 Tg/year.
630
631 *4.2 Vertical distributions in POM composition*
632 While TSS and POC concentrations increased with depth, the %OC and %N per unit
633 sediment weight decreased in all April and July 2014 profiles at Óbidos (Table 3, Fig. 2).

Bouchez et al. (2014) argued that greater associations between POC and mineral surfaces and/or greater concentration of fine carbon-rich particles from buoyant organic debris drive enrichment of POC in the surface and decreased POC loading with coarser sediments at depth. Despite the clear hydrodynamic sorting of sediment and POC concentrations in the mainstem, POC composition is less variable throughout both cross-sectional surveys in April and July 2014, and changes in C/N and carbon isotope composition ($\delta^{13}C$ and F_m) are smaller. Thus, even while depth-specific sampling may be necessary to accurately calculate POC fluxes across the mainstem, single measurements may be sufficient to understand POC composition. This also means that when comparing compositional measurements across studies, differences in sampling depth are less important than differences in sampling methodologies like pore size or, potentially, time of year.

The lack of large depth-specific variations in bulk POC composition is one likely reason that enzyme activities were homogenous throughout the cross-section at Óbidos, supporting an argument that the homogenous organic matter composition throughout the mainstem controls enzyme activities to a greater extent than do changes in particle surface area/grain size and TSS concentrations. Surprisingly, incubation studies have reported a relationship between microbial respiration rates and water velocity in Amazon River water samples (Ward et al., 2018, 2019), which do span a large range with depth (Fig. 1). However, if these enzyme activities are free-living, detached from bacterial cells in the aquatic environment, they are not likely to correlate with changes in microbial respiration in the water column (Baltar, 2018). These invariable activities do not negate the importance of particle-microbe interactions in the metabolism of organic matter in mainstem waters (Satinsky et al., 2014). Given that our results comprise the first measurement of enzyme activities in the Amazon River mainstem, we suggest further exploration of enzyme activities to understand in situ microbial dynamics in relation to sediment sorting and POC composition in the mainstem and tributaries.

There are, however, a few notable differences in POC composition across sample depths that follow the hydrodynamic models discussed in Sect. 4.1, particularly in July. We observed lower fraction modern values measured in surface POC samples and higher values measured in deeper samples at Óbidos in July 2014 (Fig. 2), which indicate a greater input of younger organic matter near the river bed compared to shallower sediments. Although the bed load sample at Óbidos still exhibits the oldest bulk carbon signature (lowest F_m) value, consistent with F_m

665 profiles in Bouchez et al. (2010), these profile data suggest an accumulation of fresher (i.e., less
666 degraded) vegetation debris just above the river bed. This is further supported by a small increase
667 (~16%) in center profile C/N ratios with depth, and an even larger increase (~40%) within
668 profiles near the right bank, implying a shift towards fresher organic matter degradation states
669 (Hedges et al., 1986).
670 Our data suggest that coarser size fractions of organic matter export fresher organic
671 matter pools, which sort vertically and are associated with higher z_R values, as observed in our
672 July 2014 Rouse fits (Sect. 4.1) (Feakins et al., 2018). By contrast, finer particle size fractions
673 carry old and/or more degraded organic matter, remaining homogenous throughout the water
674 column and yielding low z_R values in TSS profiles (Bouchez et al., 2010; Lupker et al., 2011),
675 which is especially apparent in the less variable F_m and grain size profiles in April (Fig. 2). This
676 understanding is consistent with earlier Amazon River Basin studies that typically divided
677 riverine POC between an older <63 μm "fine" fraction and a fresher >63 μm "coarse" fraction
678 (Aufdenkampe et al., 2007; Hedges et al., 1986, 1994, 2000; Richey et al., 1990). But, notably,
679 we are able to report complementary results by pooling all suspended sediment data into one
680 size-fraction (>0.2 μm), rather than into discrete size classes, assuming that organic matter
681 degradation stages are more likely to partition along a continuum of grain sizes.
682 The terrestrial leaf wax *n*-alkane data from the mainstem further supplement this
683 argument (Fig. 4). POC-normalized abundances and $\delta^{13}C$ values of chain lengths 29 and 31
684 decreased between the surface (i.e., large-volume) and deepest samples. This differentiation of *n*-
685 alkane $\delta^{13}C$ with depth fits the perspective of fresher C3 vegetation accumulating near the river
686 bed, leaving more ^{13}C-enriched leaf wax compounds at the surface from a more degraded
687 organic matter origin relative to deeper samples (Feakins et al., 2018; Häggi et al., 2016). The
688 following section elaborates on the potential sources of this degraded organic matter pool that
689 dominates the finer, well-mixed particles in the Amazon River mainstem.
690
691 *4.3 Differentiating soil organic matter sources to riverine POC*
692 This section endeavors to identify the POC pools that explain the small variations in POC
693 composition observed in depth profiles of the Amazon River mainstem. Importantly, the
694 abundances of *n*-alkanes and fatty acids measured in suspended sediment samples from various
695 depths at Óbidos underscore the influence of terrestrial vegetation in riverine POC within the

mainstem. Odd-over-even predominance of the higher chain length *n*-alkanes (C_{25}-C_{35}), even-over-odd predominance of the higher chain length fatty acids (C_{24}-C_{34}), and high ACL values of each compound class reflect input from land plants (Figs. 4c, 5, 6b) (Cranwell, 1982). Stable carbon isotope values for the long-chain *n*-alkanes and fatty acids are within range of previous long-chain *n*-alkanes and fatty acids measured across the Amazon River Basin (Feakins et al., 2018; Häggi et al., 2016) (Tables S1, S2, Figs. 4b, 6a, b). These isotope values are similar to the bulk leaf $\delta^{13}C$ composition of woody C3 plants from *terra firme* forests (average = -32.3 ‰), and roughly 4‰ more depleted than C3 leaf samples from the savannah region (average = -29.0 ‰) (Ometto et al., 2006; Powell et al., 2012; Sanaiotti et al., 2002). Notably, these offsets are smaller than previously published offsets (e.g., ~5.9 ‰ difference between *n*-alkanes and bulk C_3 leaves) (Collister et al., 1994), suggesting additional sources of ^{13}C-enriched *n*-alkanes.

Even the small presence of high elevation plants from the Andes and C4 plants from southern regions of the Amazon River floodplain could contribute ^{13}C-enriched *n*-alkanes in the mainstem (Feakins et al., 2018; Feng et al., 2016; Martinelli et al., 1994; Powell et al., 2012; Wu et al., 2017). Another reason that compound-specific $\delta^{13}C$ values are more ^{13}C-enriched than expected for fresh vegetation is that the majority of vegetation-derived POC in the Amazon River Basin enters the river via the soil organic matter reservoir, which bears a strong degraded vegetation signature (Feakins et al., 2018; Hedges et al., 1986). Indeed, long-chain (C_{24-32}) fatty acids from Óbidos in 2005 exhibited a fraction modern value of 0.83, corresponding to 1,530 radiocarbon years (Eglinton et al. 2021), implying that a significant fraction of the organic matter derived from vegetation in the mainstem POC is likely pre-aged. Feakins et al. (2018) found that the $\delta^{13}C$ values of *n*-alkanes in soils from the Madre de Dios River catchment area in the Andes were more ^{13}C-enriched due to flushing from deeper, older soil layers. If these *n*-alkanes came from atmospheric CO_2 that was fixed centuries ago, they also suggested that the Suess Effect (Ehleringer et al., 2000) could have a compound effect in raising the $\delta^{13}C$ value of older *n*-alkanes relative to modern vegetation.

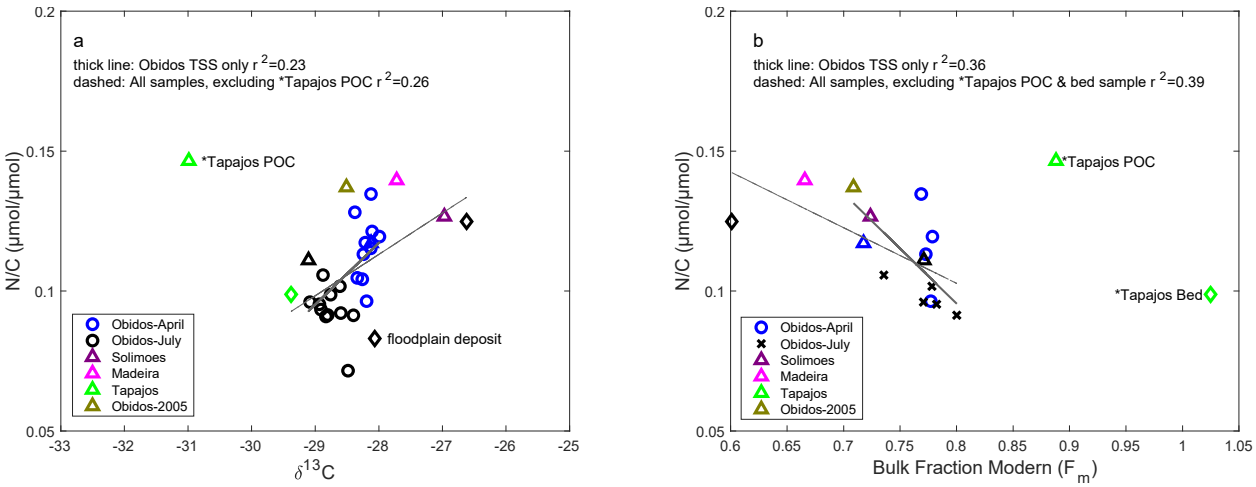

Figure 8. Bulk N/C ratios as a function of (a) $\delta^{13}C_P$ (‰) and (b) fraction modern (F_m) in samples collected in June 2005, April 2014 and July 2014. In the legend, colors are specific to location and/or time, while the symbols refer to sample type (circles for depth-specific samples, triangles for surface samples, and diamonds for bed/floodplain samples).

Adding to the argument that riverine POC is largely soil derived and pre-aged, the bulk C/N and $\delta^{13}C$ values measured for POC throughout the mainstem at Óbidos are within the range of values observed for soils across the drainage basin (Table 3, Fig. 2) (Ometto et al., 2006; Quesada et al., 2010; Sanaiotti et al., 2002). Figure 8a illustrates a weak but positive correlation between bulk N/C and $\delta^{13}C$ values measured in suspended sediments at Óbidos, highlighting a mixing relationship between a fresher, low N/C, and ^{13}C-depleted end-member and a more degraded, high N/C and ^{13}C-enriched end-member (r^2= 0.23). This mixing relationship is slightly stronger in July samples only (r^2=0.34), and when including bedload, floodplain deposit and upstream tributary samples (r^2= 0.26). Figure 8b illustrates a complementary negative relationship between bulk N/C and F_m values in the same samples (r^2= 0.36 – 0.39), supporting the perspective that these low N/C samples are indeed younger in age (higher F_m), while the high N/C samples are older (lower F_m). Two non-mutually exclusive hypotheses could account for these distinct soil-derived end-members exported by the Amazon River mainstem: (1) the mixing of several soil sources from different landscapes that bear distinct $\delta^{13}C$ signatures and degradation histories, and (2) the mixing of soils from different depth horizons throughout the drainage basin.

746 The first hypothesis makes sense considering that, while the majority of the surface area
747 covering Amazônia is dominated by ^{13}C-depleted C3 landscapes in the low-lying floodplain,
748 there are sources of more ^{13}C-enriched POC from C4 grassland ecosystems and higher altitude
749 Andean landscapes. The soil POC exported by higher elevation landscapes into the Madeira and
750 Solimões Rivers are ^{13}C-enriched relative to floodplain POC because of altitude effects
751 (Aufdenkampe et al., 2007; Feakins et al., 2018; Wu et al., 2017) and the flushing of petrogenic
752 organic carbon (Bouchez et al., 2014). To return to seasonality, this mixing of geographically
753 and isotopically diverse landscapes, both soil-derived and petrogenic, would provide one
754 explanation for the slight differences in the bulk POC composition observed at Óbidos between
755 sampling months. Lower average molar C/N ratios of 8.7 ± 0.89 in April compared to 10.8 ± 1.2
756 in July ($p<0.05$, Student's t-test) in depth-specific samples, as well as significantly more ^{13}C-
757 enriched bulk $\delta^{13}C$ values in April (-28.2 ± 0.1‰) than in July (-28.8 ± 0.2‰), suggest a small
758 shift in soil source between river stages.
759 The bulk values in July (Table 3) are consistent with increased drainage of the adjacent
760 floodplain during receding water levels, as the floodplain and várzea lakes are dominated by
761 soils replete with the residual organic carbon from C_3 plants (Quay et al. 1992; Moreira-Turcq et
762 al. 2013; Feakins et al. 2018). This enhanced exchange between the river bed and riverine POC
763 explains how the C/N ratio of suspended POC in July is closer in composition to that of the N-
764 depleted floodplain deposit sample. By contrast, the distribution of data from April 2014 imply
765 that the mainstem during rising waters is influenced by a greater proportion of POC from the
766 upstream tributaries, and is compositionally more similar to their ^{13}C-enriched and N-enriched
767 signature (Table 3, Fig. 8a). Further, the lower C/N of POC in this sampling month is consistent
768 with lower bulk F_m values and older radiocarbon ages observed for the Solimões and Madeira
769 river samples. Indeed, data from the Agência Nacional de Águas show that Solimões River
770 discharge rose from April to May 2014, while Madeira River discharge peaked in March to April
771 2014, decreasing thereafter. Increased incidence of landslides in the Andes during the months
772 leading up to April would increase the input of high altitude ^{13}C-enriched POC from these
773 tributaries to Óbidos (Clark et al., 2013), as well as the supply of old petrogenic organic carbon
774 (Bouchez et al., 2014). Thus, the preferential transport of the more degraded pools of this
775 Andean soil source to Óbidos would explain both the more degraded and ^{13}C-enriched signatures
776 of POC observed in April.

The second hypothesis could also explain the partitioning of POC in mainstem because soil organic matter across the Amazon River Basin typically gets more ^{13}C-enriched with depth within the first ~2 meters below surface, a result of microbial degradation and the Suess Effect (Ehleringer et al., 2000; Ometto et al., 2006; Sanaiotti et al., 2002). In the Amazon headwaters in the Andes, *n*-alkanes from vegetation preserved in soils were ^{13}C-enriched in deeper soil horizons (Feakins et al., 2018). This second hypothesis does not exclude the importance of riverine POC sources from different landscapes (i.e., our first mechanism, described above). But, similarly, it does explain the temporal shifts in bulk $\delta^{13}C$ and C/N values of POC at Óbidos, particularly the greater input of ^{13}C-depleted, higher C/N soil POC in July, as falling river waters draw more carbon from the superficial layers of the floodplain (Bouchez et al., 2014). Again, input of this fresher organic matter to the river in July is consistent with accumulation of higher F_m POC, possibly from coarser and less degraded vegetation debris, in the deeper sections of the river (Fig. 2).

4.4. Small influence of autochthonous organic matter in the mainstem

While floodplain lakes surrounding the mainstem have been observed to be sites of high phytoplankton and macrophyte growth, *in situ* primary production is not a significant component of riverine organic matter at Óbidos (Saliot et al. 2001; Moreira-Turcq et al. 2013). This is particularly clear when comparing to the composition of Tapajós POC, which clearly falls off the mixing line in Fig. 8a, with its high N/C and low $\delta^{13}C$ value. This observation is consistent with prior observations of Tapajós River POC composition and chlorophyll-a concentrations that imply a dominant input of *in situ* primary production (Martinelli et al., 1994; Mortillaro et al., 2011; Ward et al., 2015). The combination of a relatively deep euphotic zone depth (from low TSS concentrations) and slower water velocities in the Tapajós River, especially during the low water season, encourages greater growth of phytoplankton and cyanobacteria compared to the sediment-rich Amazon River (Mortillaro et al., 2011).

Interestingly, even-over-odd predominance of fatty acids in this sample indicates that vegetation still comprises a source of POC in the Tapajós River. A shifting balance between terrestrial POC inputs and primary production could explain observations of more ^{13}C-enriched POC collected during other months of the year (e.g., Mortillaro et al. 2011; Ward et al. 2015). But, far greater C_{16} and C_{18} abundances (23.2 ng/µg POC and 11.4 ng/µg POC, respectively)

relative to higher chain length fatty acids highlight the dominance of phytoplankton-derived organic matter in July 2014 (Mortillaro et al., 2011) (Table S2). A low fatty acid-based ACL value at the tributary surface (Fig. 6b) indicates that lower chain length lipids produced by aquatic phytoplankton contribute much more to POC in this tributary, while they are comparatively absent in POC from the mainstem and both the Solimões and Madeira Rivers upstream (Cranwell, 1982).

The radiocarbon ages measured in the Tapajós River samples are more perplexing. The Tapajós River bed sample exhibited a modern-aged F_m value of 1.02 (Table 3, Fig. 8b), supporting the perspective that fresh organic matter is indeed a source of organic material deposited on the river bed, though its $\delta^{13}C$ and C/N signature implies a terrestrial, rather than phytoplankton-derived, source (Martinelli et al., 1994; Quesada et al., 2010) (Fig. 8a). Possibly, backwashing of the Amazon River mainstem into the Tapajós River slows the river flow down enough to promote settling of coarse and fresh POC flushed in from the floodplain, complicating the inputs of river carbon to the Tapajós bedload (Fricke et al., 2017). Preferential respiration of autochthonous organic matter and burial of terrestrial POC may also contribute to the terrestrial signature of the Tapajós river bed (Bertassoli Jr et al., 2017). More importantly, suspended POC in the Tapajós River is not modern, exhibiting a surprisingly low $F_m < 0.9$ (Table 3, Fig. 8b). Assuming *in situ* fixation of DIC with a modern radiocarbon age, an age which is empirically unknown for the Tapajós River but observed elsewhere across the floodplain (Mayorga et al., 2005b), one would have expected a Tapajós POC F_m value >1, similar to the bed sample. Further analyses of the radiocarbon age distribution of bulk POC using temperature-controlled ramped pyrolysis/oxidation analysis (Hage et al., 2020; Rosenheim & Galy, 2012) could provide further insight towards the isotopically distinct POC exported by the Tapajós River.

5 Conclusions

As the world's largest river by discharge and drainage basin, the Amazon River mainstem transports over 10 Tg of particulate organic carbon (POC) per year, representing the fraction of organic carbon export with the highest likelihood of sequestration in Atlantic Ocean sediments. This quantity alone comprises 1% of the magnitude of increase in global riverine organic carbon export to the ocean during the Industrial Revolution from soil mobilization, 1 ± 0.5 Gt carbon per year (Friedlingstein et al., 2019; Regnier et al., 2013). Building upon decades of prior research, our bulk and compound-specific analyses of POC from two Óbidos surveys (2005 and 2014)

highlight that the majority of these particles are soil-derived, though input of POC from riverine algae from tributaries like the Tapajós River may be important downstream. Our approach to sampling suspended sediments from several profiles of the Amazon River cross-section show that depth-related differences in total POC concentration follow trends expected from vertical hydrodynamic sorting, supporting application of the depth-specific sampling approach to calculate export fluxes in large rivers in the Amazon River Basin.

Meanwhile, compositional differences in bulk POC and lipid isotope composition are considerably smaller, and support a perspective developed over multiple earlier studies that larger grain sizes in the river, which tend to accumulate deeper, are associated with less degraded vegetation debris, while finer grain sizes, well mixed throughout the water column, are associated with more degraded soil organic matter sources. Overall, because these vertical differences in organic matter composition are relatively small, we suggest that the depth-specific sampling approach is perhaps not essential to tracing the sources of POC exported by the Amazon River. Given the large seasonal variations in Amazon River discharge, it is possible that this conclusion is not applicable for suspended sediments from other stages of the hydrological cycle before and after the high/peak flow months, which we did not sample.

Acknowledgements

Sarah Rosengard, Rob Spencer, and Valier Galy wrote the manuscript, with input from the other co-authors. Sarah Rosengard, Robert G.M. Spencer, Valier Galy, Jose Mauro S. Moura, and Andrew Steen participated in the field work in 2014. Sarah Rosengard, Carl Johnson, Ann McNichol, and Andrew Steen analyzed the field samples. The research was funded by the Woodwell Climate Research Center, the Woods Hole Oceanographic Institution Coastal Ocean Institute grant, and the National Science Foundation Graduate Research Fellowship Program. Finally, we extend our special gratitude to Rardiles Branches, Miyuki Mitsuya, Polyana Valente, and Gabriela Vidal, students from the Universidade Federal do Oeste do Pará; our field work on the Rio Amazonas and Rio Tapajós could not have been done without them.

Open Research Statement

All discrete sample data for this research are included and tabulated in the current paper and its supplementary information files, as well as in Bouchez et al. (2011b) and Bouchez et al. (2014).

These sample data, including raw water velocity data sets obtained from the Acoustic Doppler Current Profiler, are further located in an open access (Creative Commons Attribution 4.0 International) repository on Zenodo (Rosengard, 2023). Readers may access this repository by navigating to the following DOI address their Internet browser: https://doi.org/10.5281/zenodo.8392815.

References

Aufdenkampe, A. K., Mayorga, E., Hedges, J. I., Llerena, C., Quay, P. D., Gudeman, J., Krusche, A. V, & Richey, J. E. (2007). Organic matter in the Peruvian headwaters of the Amazon: Compositional evolution from the Andes to the lowland Amazon mainstem. *Organic Geochemistry*, *38*(3), 337–364.

Baltar, F. (2018). Watch out for the "living dead": cell-free enzymes and their fate. *Frontiers in Microbiology*, *8*, 2438.

Bertassoli Jr, D. J., Sawakuchi, A. O., Sawakuchi, H. O., Pupim, F. N., Hartmann, G. A., McGlue, M. M., Chiessi, C. M., Zabel, M., Schefuß, E., & Pereira, T. S. (2017). The fate of carbon in sediments of the Xingu and Tapajós clearwater rivers, Eastern Amazon. *Frontiers in Marine Science*, *4*, 44.

Bouchez, J., Beyssac, O., Galy, V., Gaillardet, J., France-Lanord, C., Maurice, L., & Moreira-Turcq, P. (2010). Oxidation of petrogenic organic carbon in the Amazon floodplain as a source of atmospheric CO2. *Geology*, *38*(3), 255–258.

Bouchez, J., Gaillardet, J., France-Lanord, C., Maurice, L., & Dutra-Maia, P. (2011a). Grain size control of river suspended sediment geochemistry: Clues from Amazon River depth profiles. *Geochemistry, Geophysics, Geosystems*, *12*(3).

Bouchez, J., Galy, V., Hilton, R. G., Gaillardet, J., Moreira-Turcq, P., Pérez, M. A., France-Lanord, C., & Maurice, L. (2014). Source, transport and fluxes of Amazon River particulate organic carbon: Insights from river sediment depth-profiles. *Geochimica et Cosmochimica Acta*, *133*, 280–298.

Bouchez, J., Métivier, F., Lupker, M., Maurice, L., Perez, M., Gaillardet, J., & France-Lanord, C. (2011b). Prediction of depth-integrated fluxes of suspended sediment in the Amazon River: Particle aggregation as a complicating factor. *Hydrological Processes*, *25*(5), 778–794.

Chen, C. (1989). *Power law of flow resistance in open channels, manning's formula revisited*.

Clark, K. E., Hilton, R. G., West, A. J., Malhi, Y., Gröcke, D. R., Bryant, C. L., Ascough, P. L., Robles Caceres, A., & New, M. (2013). New views on "old" carbon in the Amazon River: Insight from the source of organic carbon eroded from the Peruvian Andes. *Geochemistry, Geophysics, Geosystems*, *14*(5), 1644–1659.

Collister, J. W., Rieley, G., Stern, B., Eglinton, G., & Fry, B. (1994). Compound-specific δ 13C analyses of leaf lipids from plants with differing carbon dioxide metabolisms. *Organic Geochemistry*, *21*(6–7), 619–627.

Cranwell, P. A. (1982). Lipids of aquatic sediments and sedimenting particulates. *Progress in Lipid Research*, *21*(4), 271–308.

Curtis, W. F., Meade, R. H., NORDIN JR, C. F., Price, N. B., & Sholkovitz, E. R. (1979). Non-uniform vertical distribution of fine sediment in the Amazon River. *Nature*, *280*(5721), 381–383.

Dai, A., & Trenberth, K. E. (2002). Estimates of freshwater discharge from continents: Latitudinal and seasonal variations. *Journal of Hydrometeorology*, *3*(6), 660–687.

Eglinton, G., & Hamilton, R. J. (1963). The distribution of alkanes. *Chemical Plant Taxonomy*, *187*, 217.

Ehleringer, J. R., Buchmann, N., & Flanagan, L. B. (2000). Carbon isotope ratios in belowground carbon cycle processes. *Ecological Applications*, *10*(2), 412–422.

Feakins, S. J., Wu, M. S., Ponton, C., Galy, V., & West, A. J. (2018). Dual isotope evidence for sedimentary integration of plant wax biomarkers across an Andes-Amazon elevation transect. *Geochimica et Cosmochimica Acta*, *242*, 64–81.

Feng, X., Feakins, S. J., Liu, Z., Ponton, C., Wang, R. Z., Karkabi, E., Galy, V., Berelson, W. M., Nottingham, A. T., & Meir, P. (2016). Source to sink: Evolution of lignin composition in the Madre de Dios River system with connection to the Amazon basin and offshore. *Journal of Geophysical Research: Biogeosciences*, *121*(5), 1316–1338.

Fricke, A. T., Nittrouer, C. A., Ogston, A. S., Nowacki, D. J., Asp, N. E., Souza Filho, P. W. M., da Silva, M. S., & Jalowska, A. M. (2017). River tributaries as sediment sinks: Processes operating where the Tapajós and Xingu rivers meet the Amazon tidal river. *Sedimentology*, *64*(6), 1731–1753.

Friedlingstein, P., Jones, M. W., O'sullivan, M., Andrew, R. M., Hauck, J., Peters, G. P., Peters, W., Pongratz, J., Sitch, S., & Le Quéré, C. (2019). Global carbon budget 2019. *Earth System Science Data*, *11*(4), 1783–1838.

Galy, V., Beyssac, O., France-Lanord, C., & Eglinton, T. (2008). Recycling of graphite during Himalayan erosion: A geological stabilization of carbon in the crust. *Science*, *322*(5903), 943–945.

Galy, V., Peucker-Ehrenbrink, B., & Eglinton, T. (2015). Global carbon export from the terrestrial biosphere controlled by erosion. *Nature*, *521*(7551), 204–207.

Guyot, J. L., Fillzola, N., Quintanilla, J., & Cortez, J. (1996). Dissolved solids and suspended sediment yields in the Rio Madeira basin, from the Bolivian Andes to the Amazon. *IAHS PUBLICATION*, 55–64.

Hage, S., Galy, V. V, Cartigny, M. J. B., Acikalin, S., Clare, M. A., Gröcke, D. R., Hilton, R. G., Hunt, J. E., Lintern, D. G., & McGhee, C. A. (2020). Efficient preservation of young terrestrial organic carbon in sandy turbidity-current deposits. *Geology*, *48*(9), 882–887.

Häggi, C., Sawakuchi, A. O., Chiessi, C. M., Mulitza, S., Mollenhauer, G., Sawakuchi, H. O., Baker, P. A., Zabel, M., & Schefuß, E. (2016). Origin, transport and deposition of leaf-wax biomarkers in the Amazon Basin and the adjacent Atlantic. *Geochimica et Cosmochimica Acta*, *192*, 149–165.

Hedges, J. I., Clark, W. A., Quay, P. D., Richey, J. E., Devol, A. H., & Santos, M. (1986). Compositions and fluxes of particulate organic material in the Amazon River 1. *Limnology and Oceanography*, *31*(4), 717–738.

Hedges, J. I., Cowie, G. L., Richey, J. E., Quay, P. D., Benner, R., Strom, M., & Forsberg, B. R. (1994). Origins and processing of organic matter in the Amazon River as indicated by carbohydrates and amino acids. *Limnology and Oceanography*, *39*(4), 743–761.

Hedges, J. I., Mayorga, E., Tsamakis, E., McClain, M. E., Aufdenkampe, A., Quay, P., Richey, J. E., Benner, R., Opsahl, S., & Black, B. (2000). Organic matter in Bolivian tributaries of the Amazon River: A comparison to the lower mainstream. *Limnology and Oceanography*, *45*(7), 1449–1466.

Kim, J.-H., Zell, C., Moreira-Turcq, P., Pérez, M. A. P., Abril, G., Mortillaro, J.-M., Weijers, J. W. H., Meziane, T., & Damsté, J. S. S. (2012). Tracing soil organic carbon in the lower

960 Amazon River and its tributaries using GDGT distributions and bulk organic matter
961 properties. *Geochimica et Cosmochimica Acta*, *90*, 163–180.
962 Kosuth, P., Callede, J., Laraque, A., Filizola, N., Guyot, J. L., Seyler, P., Fritsch, J. M., &
963 Guimaraes, V. (2009). Sea-tide effects on flows in the lower reaches of the Amazon River.
964 *Hydrological Processes: An International Journal*, *23*(22), 3141–3150.
965 Lupker, M., France-Lanord, C., Lavé, J., Bouchez, J., Galy, V., Métivier, F., Gaillardet, J.,
966 Lartiges, B., & Mugnier, J. (2011). A Rouse-based method to integrate the chemical
967 composition of river sediments: Application to the Ganga basin. *Journal of Geophysical*
968 *Research: Earth Surface*, *116*(F4).
969 Martinelli, L. A., Victoria, R. L., Forsberg, B. R., & Richey, J. E. (1994). Isotopic composition
970 of major carbon reservoirs in the Amazon floodplain. *International Journal of Ecology and*
971 *Environmental Sciences*, *20*(1), 31–46.
972 Mayorga, E., Aufdenkampe, A. K., Masiello, C. A., Krusche, A. V, Hedges, J. I., Quay, P. D.,
973 Richey, J. E., & Brown, T. A. (2005a). Young organic matter as a source of carbon dioxide
974 outgassing from Amazonian rivers. *Nature*, *436*(7050), 538–541.
975 Mayorga, E., Aufdenkampe, A. K., Masiello, C. A., Krusche, A. V, Hedges, J. I., Quay, P. D.,
976 Richey, J. E., & Brown, T. A. (2005b). Young organic matter as a source of carbon dioxide
977 outgassing from Amazonian rivers. *Nature*, *436*(7050), 538–541.
978 McNichol, A. P., Gagnon, A. R., Jones, G. A., & Osborne, E. A. (1992). Illumination of a black
979 box: analysis of gas composition during graphite target preparation. *Radiocarbon*, *34*(3),
980 321–329.
981 McNichol, A. P., Gagnon, A. R., Osborne, E. A., Hutton, D. L., Von Reden, K. F., & Schneider,
982 R. J. (1995). Improvements in procedural blanks at NOSAMS: reflections of improvements
983 in sample preparation and accelerator operation. *Radiocarbon*, *37*(2), 683–691.
984 Moreira-Turcq, P., Bonnet, M., Amorim, M., Bernardes, M., Lagane, C., Maurice, L., Perez, M.,
985 & Seyler, P. (2013). Seasonal variability in concentration, composition, age, and fluxes of
986 particulate organic carbon exchanged between the floodplain and Amazon River. *Global*
987 *Biogeochemical Cycles*, *27*(1), 119–130.
988 Moreira-Turcq, P., Seyler, P., Guyot, J. L., & Etcheber, H. (2003). Exportation of organic carbon
989 from the Amazon River and its main tributaries. *Hydrological Processes*, *17*(7), 1329–1344.

Mortillaro, J.-M., Abril, G., Moreira-Turcq, P., Sobrinho, R. L., Perez, M., & Meziane, T. (2011). Fatty acid and stable isotope (δ13C, δ15N) signatures of particulate organic matter in the lower Amazon River: Seasonal contrasts and connectivity between floodplain lakes and the mainstem. *Organic Geochemistry*, *42*(10), 1159–1168.

Mueller, D. S., Wagner, C. R., Rehmel, M. S., Oberg, K. A., & Rainville, F. (2009). *Measuring discharge with acoustic Doppler current profilers from a moving boat*. US Department of the Interior, US Geological Survey Reston, Virginia (EUA).

Mullen, L., Boerrigter, K., Ferriero, N., Rosalsky, J., Barrett, A. van B., Murray, P. J., & Steen, A. D. (2018). Potential activities of freshwater exo-and endo-acting extracellular peptidases in East Tennessee and the Pocono Mountains. *Frontiers in Microbiology*, *9*, 368.

Ometto, J. P. H. B., Ehleringer, J. R., Domingues, T. F., Berry, J. A., Ishida, F. Y., Mazzi, E., Higuchi, N., Flanagan, L. B., Nardoto, G. B., & Martinelli, L. A. (2006). The stable carbon and nitrogen isotopic composition of vegetation in tropical forests of the Amazon Basin, Brazil. *Biogeochemistry*, *79*(1–2), 251–274.

Powell, R. L., Yoo, E.-H., & Still, C. J. (2012). Vegetation and soil carbon-13 isoscapes for South America: integrating remote sensing and ecosystem isotope measurements. *Ecosphere*, *3*(11), 1–25.

Quay, P. D., Wilbur, D. 0, Richey, J. E., Hedges, J. I., Devol, A. H., & Victoria, R. (1992). Carbon cycling in the Amazon River: implications from the 13C compositions of particles and solutes. *Limnology and Oceanography*, *37*(4), 857–871.

Quesada, C. A., Lloyd, J., Schwarz, M., Patiño, S., Baker, T. R., Czimczik, C., Fyllas, N. M., Martinelli, L., Nardoto, G. B., & Schmerler, J. (2010). Variations in chemical and physical properties of Amazon forest soils in relation to their genesis. *Biogeosciences*, *7*(5), 1515–1541.

Regnier, P., Friedlingstein, P., Ciais, P., Mackenzie, F. T., Gruber, N., Janssens, I. A., Laruelle, G. G., Lauerwald, R., Luyssaert, S., & Andersson, A. J. (2013). Anthropogenic perturbation of the carbon fluxes from land to ocean. *Nature Geoscience*, *6*(8), 597–607.

Richey, J. E., Hedges, J. I., Devol, A. H., Quay, P. D., Victoria, R., Martinelli, L., & Forsberg, B. R. (1990). Biogeochemistry of Carbon in the Amazon River. *Limnology and Oceanography*, *35*(2), 352–371. http://www.jstor.org/stable/2837538

Richey, J. E., Meade, R. H., Salati, E., Devol, A. H., Nordin Jr, C. F., & Santos, U. Dos. (1986). Water discharge and suspended sediment concentrations in the Amazon River: 1982–1984. *Water Resources Research*, *22*(5), 756–764.

Richey, J. E., Melack, J. M., Aufdenkampe, A. K., Ballester, V. M., & Hess, L. L. (2002). Outgassing from Amazonian rivers and wetlands as a large tropical source of atmospheric CO2. *Nature*, *416*(6881), 617–620.

Rosengard, S. (2023). *Obidos 2014 - part 1 (2.0)*. [Data set]. Zenodo. https://doi.org/10.5281/ZENODO.8392815

Rosenheim, B. E., & Galy, V. (2012). Direct measurement of riverine particulate organic carbon age structure. *Geophysical Research Letters*, *39*(19).

Rouse, H. (1950). Engineering Hydraulics* John Wiley and Sons. *Inc., New York*, 414.

Saliot, A., Mejanelle, L., Scribe, P., Fillaux, J., Pepe, C., Jabaud, A., & Dagaut, J. (2001). Particulate organic carbon, sterols, fatty acids and pigments in the Amazon River system. *Biogeochemistry*, *53*, 79–103.

Sanaiotti, T. M., Martinelli, L. A., Victória, R. L., Trumbore, S. E., & Camargo, P. B. de. (2002). Past vegetation changes in Amazon Savannas determined using carbon isotopes of soil organic matter 1. *Biotropica*, *34*(1), 2–16.

Satinsky, B. M., Crump, B. C., Smith, C. B., Sharma, S., Zielinski, B. L., Doherty, M., Meng, J., Sun, S., Medeiros, P. M., & Paul, J. H. (2014). Microspatial gene expression patterns in the Amazon River Plume. *Proceedings of the National Academy of Sciences*, *111*(30), 11085–11090.

Sun, S., Schefuß, E., Mulitza, S., Chiessi, C. M., Sawakuchi, A. O., Zabel, M., Baker, P. A., Hefter, J., & Mollenhauer, G. (2017). Origin and processing of terrestrial organic carbon in the Amazon system: lignin phenols in river, shelf, and fan sediments. *Biogeosciences*, *14*(9), 2495–2512.

Ward, N. D., Keil, R. G., Medeiros, P. M., Brito, D. C., Cunha, A. C., Dittmar, T., Yager, P. L., Krusche, A. V, & Richey, J. E. (2013). Degradation of terrestrially derived macromolecules in the Amazon River. *Nature Geoscience*, *6*(7), 530–533.

Ward, N. D., Krusche, A. V, Sawakuchi, H. O., Brito, D. C., Cunha, A. C., Moura, J. M. S., da Silva, R., Yager, P. L., Keil, R. G., & Richey, J. E. (2015). The compositional evolution of

dissolved and particulate organic matter along the lower Amazon River—Óbidos to the ocean. *Marine Chemistry*, *177*, 244–256.

Ward, N. D., Sawakuchi, H. O., Neu, V., Less, D. F. S., Valerio, A. M., Cunha, A. C., Kampel, M., Bianchi, T. S., Krusche, A. V, & Richey, J. E. (2018). Velocity-amplified microbial respiration rates in the lower Amazon River. *Limnology and Oceanography Letters*, *3*(3), 265–274.

Ward, N. D., Sawakuchi, H. O., Richey, J. E., Keil, R. G., & Bianchi, T. S. (2019). Enhanced aquatic respiration associated with mixing of clearwater tributary and turbid Amazon river waters. *Frontiers in Earth Science*, *7*, 101.

Whiteside, J. H., Olsen, P. E., Eglinton, T. I., Cornet, B., McDonald, N. G., & Huber, P. (2011). Pangean great lake paleoecology on the cusp of the end-Triassic extinction. *Palaeogeography, Palaeoclimatology, Palaeoecology*, *301*(1–4), 1–17.

Wu, M. S., Feakins, S. J., Martin, R. E., Shenkin, A., Bentley, L. P., Blonder, B., Salinas, N., Asner, G. P., & Malhi, Y. (2017). Altitude effect on leaf wax carbon isotopic composition in humid tropical forests. *Geochimica et Cosmochimica Acta*, *206*, 1–17.

1066

1067